Mathematical modeling of radiation induced atherosclerosis in ApoE(-/-) mice

Author:
Maud Briels
13-01-16

Universiteit Utrecht

Rijksinstituut voor Volksgezondheid en Milieu
Ministerie van Volksgezondheid, Welzijn en Sport

Supervisors
dr. S.A.J. Dekkers (RIVM)
dr. P.A. Zegeling (UU)
Second reader
dr. T. van Leeuwen

Written in colaboration with
dr. T. van Dillen
dr. A. Kloosterman

This thesis is written at the Centre for Environmental Safety and Security (cVLH), part of the National Institute for Public Health and the Environment (RIVM).

Abstract

We consider an existing deterministic bio-mathematical model describing the initial stage of atherosclerosis, an inflammatory disease characterized by the formation of plaques within the arterial wall. Several experimental studies have suggested that irradiation of the heart or neck region by X-rays increases the risk of getting atherosclerosis. Radiation dependence is included in the model via a stochastic initiation process. We extend the deterministic growth model by incorporating the formation of a necrotic core in plaques. We present a set of differential equations which is combined with the stochastic initiation process to fit to data from irradiated mice. The model returns multiple possible growth scenario's, that require more insight in biological processes for further improvements. The actual number of plaques is under-estimated because of overlap. We present a method to model the plaque-covered area in the artery, taking the possibility of overlap into account.

Contents

Introduction **1**

1 Initial model describing the first stage in plaque growth **3**
1.1 Initial model 4
1.2 First analysis of the model 6

2 Relation of development of plaques to radiation **9**
2.1 Maximum likelihood 10

3 Extended model: adding cell death **13**
3.1 Adding apoptosis 14
3.2 Fitting the apoptosis model to data 20
3.2.1 Comparing the initial growth model with the apoptosis model 24
3.2.2 Time scales and quasi steady states 25

4 Overlapping plaques **28**
4.1 Plaques with a fixed size 29
4.2 Growing plaques 34
4.2.1 Using simulated annealing to find parameter values 35
4.2.2 Results from fitting 36

5 Discussion and conclusion **42**

A Illustration of the quasi steady state approximation **44**

B Terminology **46**

Introduction

Atherosclerosis is a chronic disease during which cholesterol accumulates in plaques in the arterial wall. The vessels narrow, eventually restricting the blood flow to organs such as the heart and lungs, which may lead to heart attacks or strokes. In the Netherlands, cardiovascular diseases have been and are the second most common cause of death according to the Dutch Heart Foundation.

Several experimental studies have demonstrated that irradiation of the heart or neck region increases the risk of getting atherosclerosis [4, 18, 17]. Given the increasing use of radiation in health care and associated burden, it is important to gain insight in how radiation promotes plaque growth. Mathematical modeling in combination with biological experiments can be used to gather understanding on the development of atherosclerosis, which in turn can help reducing the mortality from cardiovascular diseases.

In this study, we first consider an existing plaque growth model from [6, 10], which is discussed in Chapter 1. In that chapter, the biological processes playing a part in atherosclerosis are summarized and some analysis is done on the model. In [6], radiation dependence is included in the model via a stochastic initiation process as outlined in Chapter 2. We extend the model by describing the growth of a plaque after initiation, characterized by the formation of a necrotic core in plaques. In Chapter 3, we give an outline of the relevant biological processes before deriving a new set of differential equations. We test the model by fitting its solution to observational data based on the method from [6] and analyze the equations. Finally, in Chapter 4 we introduce a new way to model the coverage of a piece of artery by plaques, taking into account that they can start to overlap as they grow. The equations are evaluated using numerical simulations. Further discussion and conclusions are provided in the final chapter.

1 Initial model describing the first stage in plaque growth

Atherosclerosis is an inflammatory disease during which white blood cells and lipids accumulate in plaques in the artery walls. In [6, 10], a model to describe the growth of these plaques is discussed. In this chapter, the biological processes playing a part in atherosclerosis are described. We refer to Appendix B for a list of descriptions of the biological terms that are the most frequently used in this thesis. Next, the system of differential equations describing these processes are explained and some analysis is done on the system.

The artery walls are composed of three layers; the intima, the media and the adventitia [10]. The intima, which is where atherosclerosis starts, is separated from the bloodstream by a layer only one cell thick which is called the endothelium, see Figure 1.1. The bloodstream is called the lumen. The two main ingredients for atherosclerosis are white blood cells and low-density lipoproteins (LDL) in the blood, which are structures built up from proteins that are filled with lipids. They transfer the lipids through the blood from and to the organs. Atherosclerotic plaques start to form when there is a dysfunction of the endothelial cells, which can be caused by radiation, smoking or obesity among others [4]. This dysfunction makes it possible for the LDL particles in the bloodstream to diffuse through the endothelium into the intima, something that does not happen in a healthy artery. Once in the intima, the cholesterol oxidizes under the influence of reactive oxygen species (ROS) after which it is referred to as modified LDL or modLDL in short. Sometimes in literature it is called oxLDL, for oxidized LDL. ROS are always present in the blood, but levels rise under the influence of for example smoking and radiation. In [1], it is described how alongside the ROS, there are high levels of antioxidant content in the bloodstream which makes it unlikely for LDL particles to oxidize while in the lumen. This is in contrast to the intima, where there are no or few antioxidants and where LDL particles oxidize almost immediately. The oxidized LDL particles get trapped in the intima [1] setting of an inflammatory reaction in which the endothelium expresses adhesion molecules to which white blood cells such as monocytes and T-cells attach. The white blood cells enter the artery wall after which the monocytes differentiate into macrophages. Macrophages take up the unwanted modLDL and sectrete cytokines while doing so. Cytokines are messengers, regulating inflammatory reactions by increasing or decreasing the number of white blood cells that are attracted. The cytokines secreted by macrophages are pro-inflammatory; they attract even more monocytes. The T-cells are activated by macrophages and

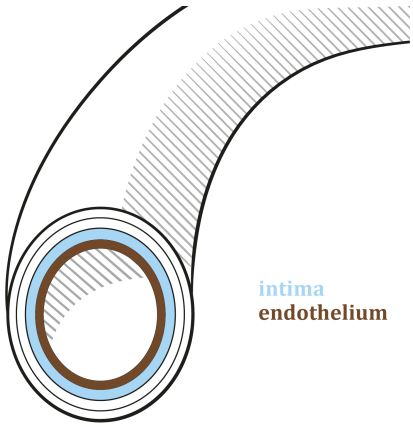

Figure 1.1: Cross section of an artery. Atherosclerosis starts in the intima after the endothelium damages.

respond to this by secreting anti- and pro-inflammatory cytokines. In the case of atherosclerosis, the attracting of white blood cells does not stop making it a chronic inflammation. The macrophages will fill up with modLDL and turn into lipid-laden foam cells. These foam cells are larger in size than empty macrophages, causing them to get stuck in the intima which is the beginning of an atherosclerotic plaque. The processes described above are schematically shown in Figure 1.2. The oxidation of LDL happens fast and is therefore not shown in this figure.

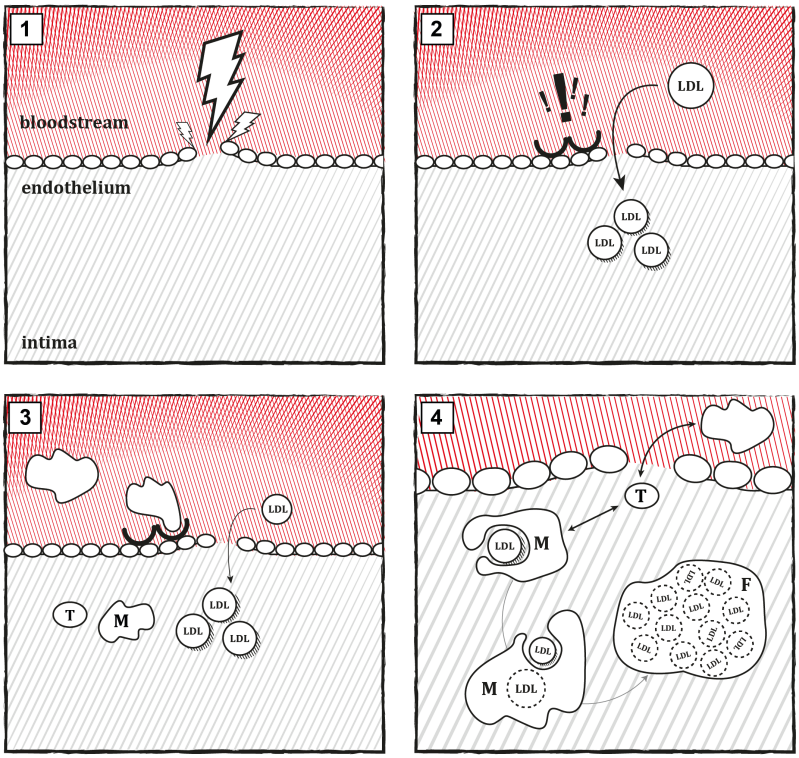

Figure 1.2: First stage of plaque development. M stands for macrophage, T for T-cells, LDL denotes modLDL particles and F stands for foam cell. 1: The endothelium gets damaged. 2: LDL enters the intima which makes that the endothelial cells attract white blood cells. 3: T-cells and macrophages enter the intima. 4: Macrophages take up the LDL particles and turn into foam cells. T-cells react to the macrophages taking up modLDL by attracting more macrophages.

1.1 Initial model

The starting point of this thesis is a model described in [6, 10]. It describes the early stage of plaque growth in atherosclerosis and we will extend it in

Chapter 3 to describe the growth of a plaque in the next stage. It is assumed that LDL particles oxidize and monocytes differentiate the moment they enter the intima and so equations for modLDL and macrophages can be considered instead of non-oxidized LDL and monocytes. In the model, given in (1.1) below, the molar concentration of modLDL particles in the artery wall is denoted by l. The variable n stands for the molar concentration of internalized lipid, meaning the modLDL particles that are ingested by macrophages. Instead of modeling macrophage concentration, the macrophage capacity concentration is considered. Capacity is denoted by m and it is defined as the amount of modLDL (in units of mol/l) that can in theory still be internalized by the macrophages in a unit volume of the artery wall. The concentration of macrophages which is denoted by M, is used to derive an equation for m in [6] and will later be used in this thesis as well. Estimates by [6] suggest that one macrophage can up in the order 10^9 modLDL particles, a quantity that is denoted by ξ. The capacity concentration then simply follows from M and n by the relation $m = \xi M - n$. Note that when lipid is ingested the capacity of the macrophages decreases, but the number of macrophages remains the same. In Table 1.1, the in- and efflux terms that should be considered are listed. Each term in the equations is discussed in more detail below.

Table 1.1: In- and efflux for the initial plaque growth model.

	influx	efflux
modLDL l	influx due to endothelial damage	uptake by macrophages
macrophages M	endothelial response to modLDL T-cell feedback	
capacity m	endothelial response to modLDL T-cell feedback	uptake of modLDL
ingested lipids n	uptake of modLDL	

$$\frac{dl}{dt} = \underbrace{F_0}_{\text{influx}} - \underbrace{\rho_1 U(l) l m}_{\text{uptake}} \tag{1.1a}$$

$$\frac{dm}{dt} = \underbrace{F_m l}_{\substack{\text{endothelial}\\ \text{response}}} + \underbrace{\rho_2 R(l,m) l m}_{\text{T-cell feedback}} - \underbrace{\rho_1 U(l) l m}_{\text{uptake}} \tag{1.1b}$$

$$\frac{dn}{dt} = \underbrace{\rho_1 U(l) l m}_{\text{uptake}} \tag{1.1c}$$

$$l(0) = l_0, \quad m(0) = m_0, \quad n(0) = n_0 \tag{1.1d}$$

In [10], different options for $U(l)$ and $R(l,m)$ are discussed and in this thesis, we use the same functions as in [6]:

$$U(l) = \frac{1}{1 + \frac{l}{l_{th}}}, \qquad R(l,m) = \frac{1}{1 + s(\frac{m}{l})^2}. \tag{1.2}$$

Oxidized LDL. The parameter F_0 stands for the constant rate of change in lipid concentration due to the influx of modLDL particles from the lumen into

the intima. The function $U(l)$ describes to what extend the macrophages take up unwanted modLDL. Basic requirements are that if l equals zero, there is no uptake while for high values of l the uptake saturates and tends to some maximum value $\rho_1 l_{th} m$. The parameter l_{th} stands for the maximum amount of modLDL that can be present in a unit volume of the artery wall. The parameter ρ_1 describes the rate of uptake per unit ingested modLDL.

Macrophage capacity. The recruitment of macrophages by the endothelium is a response to the presence of modLDL in the intima and is modeled by the term $F_m l$. Here, the parameter F_m denotes the capacity concentration influx rate caused by one unit concentration modLDL. T-cells may recruit extra macrophages as a response to the cytokines released by macrophages ingesting modLDL. If m/l is small, there is a low macrophage capacity compared to the amount of free modLDL particles and extra capacity is attracted. This is incorporated in the feedback function R. The parameter s controls the steepness of this function and should always be strictly positive. Parameter ρ_2 describes the rate of recruitment per unit of ingested modLDL particles. The macrophage capacity decreases when oxidized LDL particles are ingested. The same uptake as in the equation for modLDL is used, since the uptake process of modLDL affects the free modLDL concentration in the intima and the theoretical uptake capacity of macrophages in a identical manner.

Internalized lipids. The internalized lipids concentration increases as the free lipids concentration decreases because of uptake by macrophages, so the uptake term is used in the last equation as well. The volume of a plaque can be computed using this variable, as in this phase of plaque development the volume is built up from these foam cells only.

The existence of solutions and steady states is checked for (1.1) before we will extend the model in Chapter 2.

1.2 First analysis of the model

The first question that should be asked is whether there exist solutions to (1.1) or not. In order to answer this question, the fundamental existence theorem for nonlinear differential equations from [3, p. 42] is used.

Theorem 1.1 (Existence and uniqueness)**.** *Let Ω be an open subset of $\mathbb{R} \times \mathbb{R}^n$ and let $F : \Omega \to \mathbb{R}^n$ be continuous and locally Lipschitz continuous in the second variable. Then there is a locally defined unique solution for the initial value problem $X' = F(t, X)$, $X(0) = X_0$.*

To prove that a function satisfies the Lipschitz condition, the following lemma can be used.

Lemma 1.2. *Let Ω be an open subset of $\mathbb{R}^n$ and $f : \Omega \to \mathbb{R}$ be a differentiable function. If f has bounded partial derivatives, then it satisfies the Lipschitz condition for some $k \in \mathbb{R}_{\geq 0}$.*

Proof. Let $X_1, X_2 \in \Omega$. Define the differentiable function $g(t) = f(tX_1 + (1-t)X_2)$ for $t \in [0,1]$. The mean value theorem states that there exists a $c \in (0,1)$ such that $g'(c) = g(1) - g(0)$. Rewrite the derivative of g to find

$$g'(t) = \frac{d}{dt} f(tX_1 + (1-t)X_2) = \nabla f(tX_1 + (1-t)X_2) \cdot (X_1 - X_2). \quad (1.3)$$

It follows that

$$f(X_1) - f(X_2) = g(1) - g(0) = g'(c) = \nabla f(cX_1 + (1-c)X_2) \cdot (X_1 - X_2). \quad (1.4)$$

Since f has bounded partial derivatives, there exists some constant $k \in \mathbb{R}_{\geq 0}$ such that $k = \|\nabla f(cX_1 + (1-c)X_2)\|$. The Lipschitz condition follows when taking Euclidean norms:

$$\|f(X_1) - f(X_2)\| \leq k\|X_1 - X_2\|. \quad (1.5)$$

□

The above will be used to show that a unique solution to (1.1) exists. The domain Ω is chosen to be $I \times (-\delta, L) \times (-\delta, C) \times (-\delta, N)$ where $l_{th} > \delta > 0$ and L, C, N are positive real numbers. I is some time interval containing $t = 0$. Negative values for l, m and n do not exist, but are considered anyway in order to be able to choose $l(0) = m(0) = n(0) = 0$ as initial condition. This is done because of biological reasons, since in a healthy artery wall there are no modLDL particles and macrophages present. System (1.1) has for $X = (l, m, n)$ right hand side

$$F(t, X) = \begin{pmatrix} F_0 - \rho_1 U(l) lm \\ F_m l + \rho_2 R(l,m) lm - \rho_1 U(l) lm \\ \rho_1 U(l) lm \end{pmatrix}. \quad (1.6)$$

Note that we have chosen the domain Ω such that $(1 + l/l_{th}) > 0$ which means that $U(l)lm$ is continuous in l, m. For the feedback function $R(l,m)lm$ continuity follows immediately for $l \neq 0$. By noting that

$$R(l,m)lm = \frac{lm}{1 + s(\frac{m}{l})^2} = l^2 \frac{x}{1 + sx^2}, \qquad \text{with } x = \frac{m}{l} \quad (1.7)$$

is continuous even for x tending to negative or positive infinity, which corresponds to l tending to zero. The feedback function is continuous and so, (1.6) is continuous. Furthermore, F is differentiable with respect to l, m, n with the partial derivatives of $U(l)lm$ and $R(l,m)lm$ given by:

$$\frac{\partial}{\partial l}[Ulm] = \frac{m}{(1 + \frac{l}{l_{th}})^2}, \qquad \frac{\partial}{\partial m}[Ulm] = U(l)l, \quad (1.8a)$$

$$\frac{\partial}{\partial l}[Rlm] = m\frac{1 + 3s(\frac{m}{l})^2}{[1 + s(\frac{m}{l})^2]^2}, \qquad \frac{\partial}{\partial m}[Rlm] = l\frac{1 - s(\frac{m}{l})^2}{[1 + s(\frac{m}{l})^2]^2}. \quad (1.8b)$$

The partial derivatives of the uptake function are bounded by choice of Ω, meaning that $U(l)lm$ satisfies the Lipschitz condition. For boundedness of the partial derivatives of the feedback function, denote again $m/l = x$. For any value of x, even infinity, the fractions in (1.8b) are bounded, meaning that for

any $(l, m) \in \Omega$, the partial derivatives of the right hand side of our system are bounded.

$$m\frac{1+3sx^2}{(1+sx^2)^2}, \qquad l\frac{1-sx^2}{(1+sx^2)^2} \tag{1.9}$$

It follows that (1.6) satisfies the Lipschitz condition, so there exists a locally defined unique solution to the model (1.1).

The next step in our analysis of a model is to verify whether it has non-trivial steady states. If it is possible to describe under what conditions the time derivatives equal zero then we find conditions under which the inflammatory process will not escalate. This means that a plaque will not grow and thus that the artery wall will stay healthy. In the case of a steady state, there is an $\widetilde{X}$ such that $F(t, \widetilde{X}) = 0$ with F defined as in (1.6). From $F_1(t, X) = 0$ it follows that $F_0 = \rho_1 U(l) lm$, but from $F_3(t, X) = 0$ we deduce that $\rho_1 U(l) lm = 0$. These two conditions contradict each other unless $F_0 = 0$, which would mean that there is no influx of modLDL at all and thus that the plaque would not start to form at all. It is however possible to determine parameter values such that $F_1(t, X)$ and $F_2(t, X)$ are equal to zero. This would correspond to a linearly growing plaque since then we would have for the internalized lipid equation $F_3(t, X) = \rho_1 U(l) lm = F_0$. From $F_1(t, X)$ follows that

$$F_1(t, X) = 0 \;\Rightarrow\; m(l) = \frac{F_0}{\rho_1 U(l)}. \tag{1.10}$$

Solving $F_2(t, X) = 0$ gives

$$\begin{aligned} -F_0 + F_m l + \rho_2 \frac{lm}{1 + s(m/l)^2} \;&=\; 0 \\ \Rightarrow\; m(l) \;&=\; \frac{-\rho_2 l \pm \sqrt{(\rho_2 l)^2 - 4s/l^2(-F_0 + F_m l)^2}}{2s/l^2(-F_0 + F_m l)}. \end{aligned} \tag{1.11}$$

The fixed value for l can be found by (1.10) and (1.11), from which m can be determined. In (1.11), the determinant $D = (\rho_2 l)^2 - 4s/l^2(-F_0 + F_m l)^2$ should be greater than or equal to zero in order to have real m. Since $4s/l^2(-F_0 + F_m l)^2 \geq 0$ is $\sqrt{D} \leq \rho_2 l$ and so the denominator of (1.11) has to be strictly negative in order to have positive m. This gives the following condition on l:

$$l < \frac{F_0}{F_m}. \tag{1.12}$$

The determinant is positive when

$$\begin{aligned} \rho_2 l \;&\geq\; -2\sqrt{s}/l^2(-F_0 + F_m l) \\ \Rightarrow\; l \;&\geq\; \frac{-\sqrt{s}F_m + \sqrt{sF_m^2 + 2\sqrt{s}\rho_2 F_0}}{\rho_2}. \end{aligned} \tag{1.13}$$

The last two conditions determine whether it is possible to find a real positive fixed value for l and m; if the expression in (1.12) is smaller than the expression in (1.13), there is no solution and so plaques grow faster than linearly.

2 Relation of development of plaques to radiation

Various studies indicate that high dose radiation can play a role in atherosclerosis. Epidemiological studies concerning cancer patients who were treated with radiotherapy for left-sided breast cancer or Hodgkin's disease have shown that radiation is a risk factor for development of cardiovascular diseases [4, 18]. Also studies among atomic bomb survivors in Japan have shown a possible relationship between radiation and heart disease [17]. Radiation may cause inflammatory reactions which can have an effect on the structure of the artery and can increase the vascular permeability. This makes it possible for LDL particles and monocytes to enter the intima promoting the inflammatory reaction described in Chapter 1 [18]. The role of low dose radiation is less clear. In [6], the effect of high dose acute radiation on the initiation and progress of atherosclerosis in mice is tested using the system of differential equations given by (1.1). The method and results from the article [6] will be discussed here before the model is extended in Chapter 3.

The data that were used in [6] and in Chapter 3 is taken from [4]. In the experiment, genetically modified mice were irradiated with 0, 8 or 14 Gray (Gy) X-ray around the age of thirteen weeks. This specific kind of mice, ApoE(-/-) mice, develops plaques with characteristics similar to human plaques [9]. Per dose group, there were ten to twelve animals. The sham group (0 Gray) was treated exactly the same as the other groups, meaning that they were also moved to the X-ray machine but without receiving an actual dose. This is done to rule out the effects of stress caused by moving the mice. Around the age of ten months they were sacrificed in order to measure the area covered by plaques in the carotid arteries. A first look at the data shows that the sizes of the atherosclerotic plaques do not differ significantly for irradiated and non-irradiated mice. The number of plaques however does differ, as is shown in Table 2.1 and Figure 2.1. It is therefore assumed that the acute irradiation has little or no effect on the growth of the plaques but does have an effect on the initiation of plaques. It might be possible though that chronic radiation has a more pronounced effect on growth of plaques.

Plaque initiations are modeled using a non-homogenous Poisson process. The effect of acute, one time only radiation on initiations disappears after approximately two weeks after the time of irradiation t_i, meaning that the plaque initiation rate is elevated for two weeks following the irradiation and then drops back to the background initiation rate. This is described in [18]. The time window of approximately 14 days is denoted by τ. The Poisson process is

Table 2.1: Area in mm^2 and number of plaques per dose group. Each dose group has ten to twelve mice. Doses are in Gray (Gy).

	mean area	min area	max area	mean nr.	min nr.	max nr.
0 Gy	0.1485	0.00262	0.5988	2.7	0	5
8 Gy	0.1636	0.0114	0.5632	4.6	1	7
14 Gy	0.1501	0.01345	0.4885	5.4	4	8

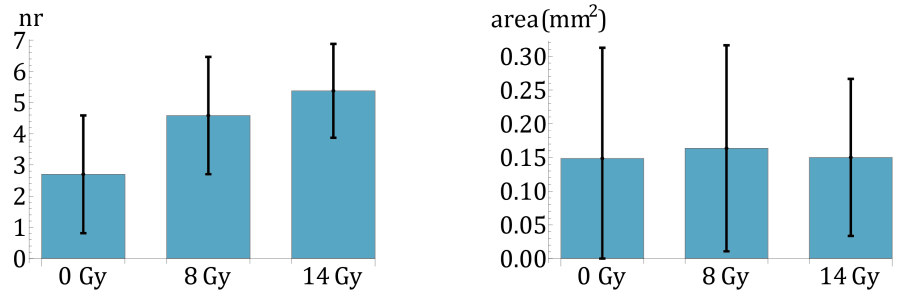

Figure 2.1: Mean values and standard deviation of the numbers and the area of plaques per dose group.

described by the following event rate

$$\lambda(t) = \lambda_0(1 + \alpha D[H(t - t_i) - H(t - t_i - \tau)]), \tag{2.1}$$

with H the Heaviside step function. The parameter D describes the dose of the irradiation and λ_0 is the baseline event rate, i.e. the rate at which plaques form without radiation. From the Poisson process, a likelihood function can be derived and this can be used to compare the data with the model. In the next section, the concept of likelihood functions is explained briefly and the likelihood function for this specific model is derived.

2.1 Maximum likelihood

The maximum likelihood method can be used to estimate unknown parameters in a random process. Let a random variable X behave according to some stochastic model with one or multiple unknown parameters π. For a fixed data set of n independent observations $X_{obs} = \{x_1, \ldots, x_n\}$, the maximum likelihood method is used to find the parameter value π_{mle} for π which makes the set of observations most probable to occur. This is done by defining a likelihood function ℓ that returns for a given value of π how likely it is to observe X_{obs}. This likelihood function is equal to the probability of finding X_{obs} given a certain value for π, as defined below. The function is then maximized in order to find π_{mle}.

$$\pi_{mle} = \max_{\pi} \ell(\pi \mid X_{obs}) = \max_{\pi} P(X_{obs} \mid \pi) = \max_{\pi} \prod_{i=1}^{n} P(x_i \mid \pi) \tag{2.2}$$

It has great computational advantages to minimize the negative $\log(\ell)$ instead of maximizing ℓ. The maximum likelihood method becomes less suitable for models with many unknown parameters in comparison with the number of variables. The more parameter values are unknown, the more general the model becomes. When a model gets too general, it is possible to describe any data set. Furthermore, the method is less efficient if the number of observations n is small, since then it is difficult to identify the effect of parameters on the random variable. There are numerous books describing the maximum likelihood method, of which we refer to [2, ch. 5]. Next, a likelihood function is derived in order to

fit the mouse plaque size data to the stochastic initiation of plaques using the deterministic growth curve from (1.1).

For the fitting process described below, the parameters in the deterministic model (1.1) are denoted by a vector β and θ denotes the parameters of the random initiation process given by (2.1). When fixing values for the parameters β, the growth curve $V(t|\beta)$ of the plaque volume follows from (1.1) by stating $V = \kappa \cdot n$. Here, κ is a parameter that transforms the molar concentration of internalized lipids into volume of internalized lipids per control volume. Now, let a mouse have its time of birth at $t = 0$ and time of death at $t = T$. Let it have n plaques with sorted observed areas $\{\widetilde{A}_1, \ldots, \widetilde{A}_n\}$ at the time of death. We assume that every plaque has the same deterministic growth curve defined by the system described in Chapter 1. The observed values in the data set describe plaque area instead of volume and so to use the data, the estimation $\widetilde{V} \approx \widetilde{A}^{3/2}$ is used. The set of observed areas is transformed to a set of volumes $\{\widetilde{V}_1, \ldots, \widetilde{V}_n\}$. The unknown initiation time for plaque i is denoted by t_i. From the growth curve V and an observed volume, it is possible to compute an expectation of how long a plaque has been developing. For plaque i, the expected initiation time is then given by

$$t_i = T - V^{-1}(\widetilde{V}_i \mid \beta), \tag{2.3}$$

where $V^{-1}(\widetilde{V}_i \mid \beta)$ is the expected growth time of a plaque which follows from the inverse growth function V^{-1} evaluated at the observed plaque volume $\widetilde{V}_i$. Since the volume of a plaque strictly increases after initiation, t_i is unique. The initiation times are ordered according to the plaque sizes; for $\widetilde{V}_i > \widetilde{V}_j$ we find $t_i < t_j$. For every plaque, an initiation time can be computed resulting in a set $S_n = \{t_i \mid i = 1, \ldots, n\}$. For this set, a likelihood function is computed. This means that $P(S_n \mid \beta, \theta)$, the probability of having exactly n plaque initiations at times $t_1, \ldots, t_n$ depending on β and θ, has to be found. This is done by discretizing the time in steps Δt, computing the probability and then finally by taking the limit of $\Delta t \to 0$.

Denote $N_{t,t+\Delta t}$ for the number of initiations in the time interval $[t, t+\Delta t]$ and $\Lambda_{t,t+\Delta t} = \int_t^{t+\Delta t} \lambda(s)ds$ for the integrated event rate, which equals the expected number of initiations in this time interval. For a Poisson process, the probability of k events occurring in a time interval $[t, t + \Delta t]$ equals

$$P(N_{t,t+\Delta t} = k) = \frac{(\Lambda_{t,t+\Delta t})^k}{k!} \exp(-\Lambda_{t,t+\Delta t}). \tag{2.4}$$

The expression above with $k = 0, 1$ is used to compute the probability of having one initiation in $[t_i, t_i + \Delta t]$ and having no new initiation up till time t_{i+1}, which is given by

$$\begin{aligned} P(N_{t_i,t_i+\Delta t} = 1) \cdot & P(N_{t_i+\Delta t,t_{i+1}} = 0) \\ &= [\Lambda_{t_i,t_i+\Delta t} \exp(-\Lambda_{t_i,t_i+\Delta t})] \cdot \left[\exp(-\Lambda_{t_i+\Delta t,t_{i+1}})\right] \\ &= \Lambda_{t_i,t_i+\Delta t} \cdot \exp(-\Lambda_{t_i,t_{i+1}}). \end{aligned} \tag{2.5}$$

Taking the limit of Δt tending to zero in (2.5) gives the probability of having an

initiation at exactly t_i and no other up till t_{i+1}.

$$\begin{aligned} &P(\text{init. at } t_i)\cdot P(\text{no init. in } (t_i, t_{i+1})) \\ &\qquad = \lim_{\Delta t\to 0} \frac{P(N_{t_i,t_i+\Delta t}=1)\cdot P(N_{t_i+\Delta t,t_{i+1}}=0)}{\Delta t} \\ &\qquad = \exp(-\Lambda_{t_i,t_{i+1}})\cdot \lim_{\Delta t\to 0}\frac{\Lambda_{t_i,t_i+\Delta t}}{\Delta t} \end{aligned} \tag{2.6}$$

We use expression (2.6) to find the probability $P(S_n \mid \beta, \theta)$. Below, t_{n+1} stands for T.

$$\begin{aligned} P(S_n|\beta,\theta) &= P(\text{no init. in } (0,t_1))\cdot\prod_{i=1}^{n} P(\text{init. at } t_i)\cdot P(\text{no init. in } (t_i,t_{i+1})) \\ &= \exp(-\Lambda_{0,t_1})\cdot\prod_{i=1}^{n}\exp(-\Lambda_{t_i,t_{i+1}})\cdot\lim_{\Delta t\to 0}\frac{\Lambda_{t_i,t_i+\Delta t}}{\Delta t} \\ &= \exp(-\Lambda_{0,T})\cdot\prod_{i=1}^{n}\lim_{\Delta t\to 0}\frac{\Lambda_{t_i,t_i+\Delta t}}{\Delta t} \end{aligned} \tag{2.7}$$

Each limit in the last line in (2.7) above is the derivative of the integrated event rate $\Lambda(t)$.

$$\lim_{\Delta t\to 0}\frac{\Lambda_{t_i,t_i+\Delta t}}{\Delta t} = \lim_{\Delta t\to 0}\frac{\Lambda_{0,t_i+\Delta t}-\Lambda_{0,t_i}}{\Delta t} = \frac{d}{dt}\Lambda_{0,t}\bigg|_{t=t_i} = \lambda(t_i) \tag{2.8}$$

This shows that, using (2.7), the likelihood function for one mouse with observed plaque volumes $\{\widetilde{V}_1,\ldots,\widetilde{V}_n\}$ equals

$$\ell(\beta,\theta) = P(S_n \mid \beta,\theta) = \exp(-\Lambda_{0,T})\prod_{i=1}^{n}\lambda(t_i) \tag{2.9}$$

with t_i given by (2.3). The parameters β are incorporated in the times t_i via the growth curve and parameters θ can be found in Λ and λ.

If an experiment consist of tests on $j = 1\ldots N$ mice, each with its own number of plaques n_j, time of death T_j and likelihood function ℓ_j, the total likelihood is given by

$$\mathcal{L}(\beta,\theta) = \prod_{j=1}^{N}\ell_j(\beta,\theta) = \prod_{j=1}^{N}\left(\exp(-\Lambda_{0,T_j})\prod_{i=1}^{n_j}\lambda(t_{i,j})\right). \tag{2.10}$$

This likelihood function should be maximized with respect to the parameter sets β,θ in order to find a solution set which describes the growth and initiation of plaques fitting to the data. This is equivalent to minimizing the negative of the ln-likelihood.

$$LLH(\beta,\theta) = -\ln\mathcal{L}(\beta,\theta) = \sum_{j=1}^{N}\Lambda_{0,T_j} - \sum_{j=1}^{N}\sum_{i=1}^{n_j}\ln\lambda(t_i) \tag{2.11}$$

Results of fitting the data to model (1.1) in Chapter 1 using the likelihood method described above are discussed in [6]. The same method will be used to test a new model that is derived in Chapter 3.

3 Extended model: adding cell death

The early plaque growth model from Chapter 1 returns a rapidly growing function for the internalized lipids n (plots are shown in Section 3.2.1). Plaque volumes are assumed to be proportional to the internalized lipid concentration, so as $\kappa \cdot n$ where κ is some constant of proportionality. In later stages, plaques often contain a core composed of dead cells, lipid deposits and cellular debris [15] and a cap of muscle cells can form around the plaque which may or may not rupture [10]. The volume of a plaque will not be built up from n only, but also a necrotic core contributes to the volume. The rupturing of plaques is dangerous because plaque content can end up in the blood stream, which can block the artery or smaller blood vessels. Our goal is to extend the plaque growth model by including the formation of this core of necrotic material.

An important process in the formation of a necrotic core is apoptosis, which is a programmed form of cell death. Under normal conditions, apoptosis is a controlled process that is initiated by the cells itself. In [7, 12, 13] it is described that during this process, the cell shrinks and condensates and the nucleus breaks up. The cell membrane starts to deform and small envelopes filled with cell content are separated from the cell, a process that is called budding. The small envelopes are called the apoptotic bodies (AB's). The apoptotic bodies are removed by a process which is called phagocytosis, in which cleaning cells such as macrophages enclose unwanted particles in order to remove them. Apoptosis, followed by phagocytosis, is a clean way of removing cells and the apoptotic bodies are rapidly removed. Apoptosis, when triggered by signals such as ionizing radiation or oxidized lipids, is often more acute compared to initiation by the body itself. In atherosclerosis, foam cells go through apoptosis because of the fact that the ingested lipids are oxidized which makes them toxic for cells that take them up [7, 12, 15]. If death of foam cells happens too fast for the cleaning cells to remove all apoptotic bodies, debris that has not been phagocytosed may rip and its contents are released into the plaque. This process is called secondary necrosis and the released contents will form the necrotic core [7, 15, 16]. Besides the fact that there are too many apoptotic bodies to clean, there is also the presence of modLDL that has not yet been ingested that influences the phagocytosis. The surface of the apoptotic bodies resembles the surface of modLDL particles, which makes that cleaning particles that should clear the apoptotic bodies also take up modLDL. This means that there is a competition between modLDL and the remains of the apoptotic foam cells [7, 15]. The leakage of cell content from apoptotic bodies into the plaque also has inflammatory effect [7, 13].

In Figure 3.1, the processes described above are depicted schematically. In Section 3.1, we discuss how the death of cells and the formation of a necrotic core can be modeled. The resulting system of differential equations is tested, compared to the initial growth system and then analyzed in Section 3.2.

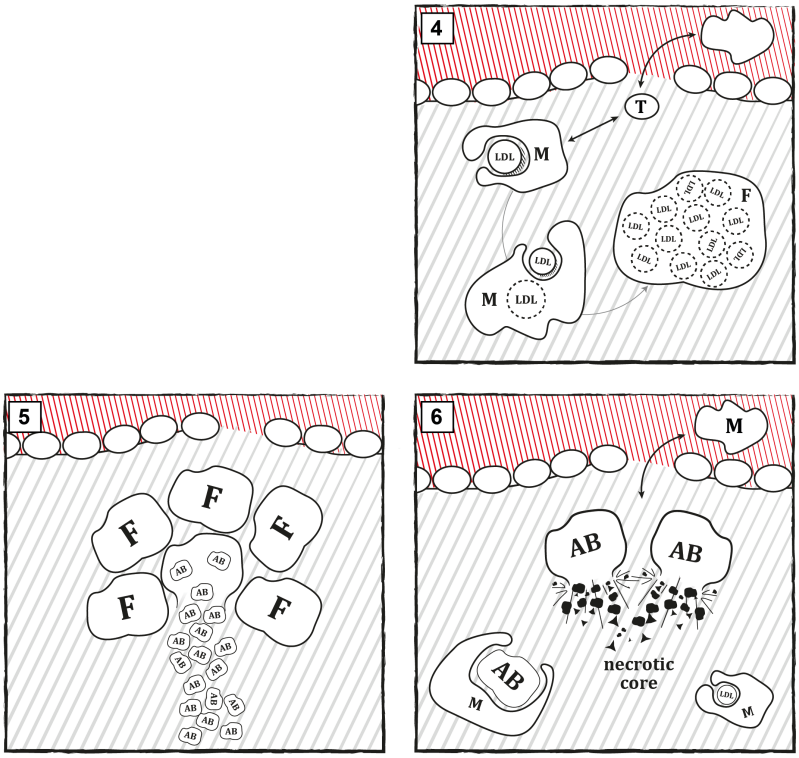

Figure 3.1: Formation of a necrotic core after the first stage of plaque development. F stands for foam cells. AB denotes apoptotic bodies. M,T and LDL are as in Figure 1.2. 4: Macrophages take up the LDL particles and turn into foam cells. T-cells react to the macrophages taking up modLDL and attract more macrophages. 5: Foam cells undergo apoptosis and break up in AB's. Be reminded that one AB contains many modLDL particles. 6: Macrophages clear AB's and modLDL particles. AB's that are not engulfed undergo secondary necrosis.

3.1 Adding apoptosis

We will add a new equation to (1.1) to incorporate apoptosis of foam cells. Again, a distinction between free modLDL and internalized lipids is made. The variables l, m, M and n are still used for the concentrations of free modLDL, macrophage uptake capacity, macrophages and internalized lipids respectively. A variable a for molar concentration of apoptotic body content is added and will be used to derive the equations. From the equation for a, an equation for molar concentration of necrotic core content c follows. Again, ξ is used to denote the approximate modLDL uptake capacity of one macrophage. Some terms in the original model stay the same, some are changed and some new ones are added.

Since apoptosis and subsequent phagocytosis typically occurs at a time scale of hours [13], we assume that the apoptosis, in our plaque growth time scale of

days, is instantaneously followed by either phagocytosis or if the phagocytosis fails by secondary necrosis. These large time scale differences will be discussed later in Section 3.2.2. We assume that apoptotic bodies that are not cleared end up in the necrotic core. The apoptotic bodies that are cleared are removed from the plaques and will not contribute to the plaque volume anymore. We also assume that on average all macrophages are either busy cleaning modLDL or cleaning apoptotic bodies, so there are no inactive macrophages. Which one of modLDL or AB's is cleaned by one particular macrophage depends on a competition between the two. Little information is available about how the competition works, so we here assume that it depends on the ratio between modLDL concentration and the concentration of apoptotic bodies. We suspect that the size of AB's compared to the size of modLDL particles, the number of receptors on the surface of the particles and the ability to move around in the artery wall also play a part in the competition. How we incorporate these uncertainties in the model is explained later in this chapter. Since apoptotic bodies are considerably larger than modLDL particles and since macrophages in plaques generally take up only one AB [14], we assume that only macrophages that are not filled up with modLDL can absorb apoptotic bodies. In reality, macrophages taking up AB's do not have to be completely empty and likewise, macrophages undergoing apoptosis have not necessarily taken up ξ modLDL particles. In our model however, we use "empty" and "full" as criteria for macrophages.

The effects of apoptosis of foam cells are modeled as follows. First, foam cells which are full macrophages fall apart and internalized lipid ends up in apoptotic bodies, resulting in a decrease in n and M and a concomitant increase in a. Note that a cell undergoing apoptosis affects the macrophage concentration M but not the macrophage capacity m, since only macrophages that are assumed to be full and thus have no capacity left undergo apoptosis. The macrophage capacity is only changed in case of uptake of either modLDL or AB's. The apoptotic process has no further effects on the capacity m. The apoptotic bodies are partly removed by empty macrophages (phagocytosis) which hence leads to a decrease in macrophages M and a. Second, apoptotic debris that is not taken up and cleared by macrophages remains in the plaque volume and becomes a part of the necrotic core, which yields an increase in c. Apoptosis has an inflammatory effect

Table 3.1: In- and efflux for the model with apoptosis incorporated.

	Influx	Efflux
modLDL l	influx	uptake by macrophages
macrophages M	endothelial response to modLDL T-cell feedback influx due to AB's	foam cell apoptosis phagocytosis
capacity m	endothelial response to modLDL T-cell feedback influx due to necrosis	uptake of modLDL phagocytosis
ingested lipids n	uptake of modLDL	foam cell apoptosis
apoptotic bodies a	foam cell apoptosis	phagocytosis secondary necrosis
necrotic core c	secondary necrosis	

meaning that extra macrophages are recruited and an increase in M should be modeled. The uptake of oxidized lipids is adjusted to incorporate the competition between modLDL and AB's. Since macrophages can ingest modLDL or AB's, two different uptake terms should be incorporated in the macrophage capacity equation. The in- and efflux terms that should be considered are listed in Table 3.1.

Apoptosis. When modeling apoptosis, it should in principle be taken into account that the uptake of modLDL is a random and spatially heterogeneous process, the latter because of how a plaque is build up. There will be less macrophage activity close to the core than at the outer region of the plaque. This makes it difficult to express the remaining capacity of a macrophage and whether it is subjected to apoptosis. We therefore do not incorporate spatial aspects in our model. Instead, the average overall occupation of the macrophages is defined to be the ratio between internalized lipids and the total amount of lipids that can be internalized; $n/(\xi M)$, a fraction that is always between 0 and 1. When there is a high overall occupation, the probability of a macrophage to be almost full and thus to break into pieces is large. The degree of occupation $n/(\xi M)$ is therefore used as probability for a macrophage to fall apart and it estimates what fraction of the macrophages is expected to undergo apoptosis. We introduce the parameter ρ_3 which is the apoptosis rate per day. Note that for every macrophage that undergoes apoptosis, approximately ξ internalized lipids are released into apoptotic bodies. The change in number of macrophages caused by apoptosis, $(dM/dt)_a$, and the change in number of internalized lipids caused by apoptosis, $(dn/dt)_a$, can now be modeled as in (3.1). The increase in a caused by apoptosis,$(da/dt)_a$, equals the decrease in internalized lipids $(dn/dt)_a$. Note that a does not express the number of apoptotic bodies but the concentration of lipids that end up in apoptotic bodies.

$$\left(\frac{dM}{dt}\right)_a = -\rho_3 M \frac{n}{\xi M}, \qquad \left(\frac{dn}{dt}\right)_a = \xi \cdot \left(\frac{dM}{dt}\right)_a = -\rho_3 n,$$
$$\left(\frac{da}{dt}\right)_a = \rho_3 n \tag{3.1}$$

Competition. Since in the new model, macrophages can engulf oxidized LDL and AB's, two different uptake functions have to be defined in which the competition between modLDL and apoptotic bodies is considered. As explained earlier, we do not know exactly how this competition works, but we assume that it mainly depends on the ratio between l and AB concentration, the latter being proportional to a. To include the uncertainty that we have about the competition, we introduce a dimensionless parameter ϵ that we refer to as the competition parameter. Now we define the probability for a macrophage to engulf modLDL, P_l, or AB's, P_a, as

$$P_l = \frac{1}{1+\epsilon\frac{a}{l}}, \qquad P_a = \frac{1}{1+\frac{1}{\epsilon}\frac{l}{a}}. \tag{3.2}$$

The given probabilities satisfy the assumption that a macrophage is always active, either engulfing l or AB's, since $P_l + P_a = 1$. As we desire, $P_l \to 0$ as $l \to 0$ and $P_a \to 0$ as $a \to 0$, reflecting the fact that no modLDL particles or

AB's are engulfed if they are not present. These probabilities will be used to define the two uptake functions.

modLDL. Neither apoptosis nor secondary necrosis influences the number of lipids that move into the artery wall. The influx term from the original model is therefore kept. In the new model, the uptake of modLDL particles depends on the competition between free oxidized lipids and apoptotic bodies and the presence of m and l. We use $P_l \cdot m$ for the fraction of macrophage capacity that is expected to be available for the uptake of modLDL particles. In the original model, a saturation term was incorporated in the uptake function (expressed as l_{th}) but in the new equation we drop this term for simplicity. The new uptake term is the product of the free oxidized lipid concentration and the concentration of macrophage capacity available for modLDL. Like in the original model, ρ_1 denotes the uptake speed.

$$\frac{dl}{dt} = \underbrace{F_0}_{\text{influx}} \underbrace{- \rho_1 \frac{1}{1+\epsilon\frac{a}{l}} lm}_{\text{uptake of } l} \tag{3.3}$$

Macrophages. Apoptosis of foam cells does not affect the recruitment of macrophages by endothelial cells as a reaction to the presence of modLDL. We assume that it neither influences the T-cell feedback, so all influx terms from the original model are used. We add two efflux terms, one for apoptosis and one for phagocytosis. Apoptosis of full macrophages is modeled as discussed above in (3.1). Phagocytosis of apoptotic bodies affects both M and m, since macrophages that ingest apoptotic bodies are removed. We use the probability P_a of a macrophage engulfing apoptotic debris as was derived in (3.2). The dependence on macrophages with enough capacity left is modeled using the overall occupation $n/\xi M$. This gives $(1 - n/\xi M) \cdot M$ for the expected number of macrophages that are available, meaning empty enough, for phagocytosis. This results in a product of probabilities, the probability that a macrophage is not full multiplied by the probability that a macrophage is engulfing a, P_a. The dependence on presence of apoptotic bodies is added and the parameter ρ_4 is introduced for the phagocytosis speed per pair of macrophages and apoptotic bodies. Next to the new efflux terms, there is one new influx term for the inflammatory effect of the apoptotic bodies. The parameter F_A is introduced to denote the speed of macrophage recruitment resulting from the presence of AB.

$$\begin{aligned}\frac{dM}{dt} = \underbrace{F_M l}_{\substack{\text{endothelial}\\ \text{response}}} + \underbrace{\widetilde{\rho_2} R(l,m) lm}_{\text{T-cell feedback}} - \underbrace{\rho_3 M \frac{n}{\xi M}}_{\text{apoptosis}} \\ \underbrace{- \rho_4 \frac{1}{1+\frac{1}{\epsilon}\frac{l}{a}} \left(1 - \frac{n}{\xi M}\right) Ma}_{\text{phagocytosis}} + \underbrace{F_A a}_{\substack{\text{inflammation}\\ \text{due to AB's}}}\end{aligned} \tag{3.4}$$

An equation for macrophage capacity can be derived from this equation, using the relation $m = \xi M - n$. Note that here, ξF_M equals F_m and $\xi\widetilde{\rho_2}$ equals ρ_2 from (1.1). Denote in the same fashion $\xi F_A = F_a$.

Internalized lipids. Since in the new model macrophages can fall apart and lose internalized lipids in the process, there is an efflux term as derived in (3.1) in addition to the uptake of modLDL that was already used in the original model. The uptake of l is adjusted and the apoptosis is added according to (3.1).

$$\frac{dn}{dt} = \underbrace{\rho_1 \frac{1}{1+\epsilon\frac{a}{l}} lm}_{\text{uptake of } l} - \underbrace{\rho_3 n}_{\text{apoptosis}} \tag{3.5}$$

Macrophage capacity. Combining (3.4) and (3.5) using the relation $m = \xi M - n$ gives a differential equation for the macrophage capacity.

$$\begin{aligned}\frac{dm}{dt} = F_m l + \rho_2 \frac{1}{1+s(\frac{m}{l})^2} lm + F_a a \\ \underbrace{-\rho_1 \frac{1}{1+\epsilon\frac{a}{l}} lm - \rho_4 \frac{1}{1+\frac{1}{\epsilon}\frac{l}{a}} am}_{\text{competition between uptake of } l \text{ and } a}\end{aligned} \tag{3.6}$$

Apoptotic bodies content. The concentration of apoptotic bodies increases when foam cells undergo apoptosis. A term to describe this is derived in (3.1). We do not know the number of apoptotic bodies but we do know the amount of n ending up as a. The clearance of a by macrophages (phagocytosis) is modeled as derived in the differential equation for m. Also the secondary necrosis has to be modeled. Since this is an inevitable event for AB's that are not cleared, we model it to be proportional to the apoptotic body content. The parameter ρ_5 is introduced for the rate of necrosis. A differential equation for apoptotic bodies follows.

$$\frac{da}{dt} = \underbrace{\rho_3 n}_{\text{apoptosis}} \underbrace{- \rho_4 \frac{1}{1+\frac{1}{\epsilon}\frac{l}{a}} am}_{\text{phagocytosis}} - \underbrace{\rho_5 a}_{\text{necrosis}} \tag{3.7}$$

Necrotic core content. The equation for necrotic core content follows directly from the equation for apoptotic bodies. The decrease in a by necrosis equals the increase in c.

$$\frac{dc}{dt} = \underbrace{\rho_5 a}_{\text{necrosis}} \tag{3.8}$$

Resulting model. All together, the new model with apoptosis incorporated is as follows.

$$\frac{dl}{dt} = F_0 - \rho_1 \frac{lm}{1+\epsilon\frac{a}{l}} \tag{3.9a}$$

$$\frac{dm}{dt} = F_m l + \rho_2 \frac{lm}{1+s(m/l)^2} + F_a \cdot a - \rho_1 \frac{lm}{1+\epsilon\frac{a}{l}} - \rho_4 \frac{am}{1+\frac{1}{\epsilon}\frac{l}{a}} \tag{3.9b}$$

$$\frac{dn}{dt} = \rho_1 \frac{lm}{1+\epsilon\frac{a}{l}} - \rho_3 n \tag{3.9c}$$

$$\frac{da}{dt} = \rho_3 n - \rho_4 \frac{am}{1+\frac{1}{\epsilon}\frac{l}{a}} - \rho_5 a \tag{3.9d}$$

$$\frac{dc}{dt} = \rho_5 a \tag{3.9e}$$

$$l(0) = l_0, \;\; m(0) = m_0, \;\; n(0) = n_0, \;\; a(0) = a_0, \;\; c(0) = c_0 \tag{3.9f}$$

To check whether the new system is well defined, we verify the smoothness of the new and adjusted terms. The term describing apoptosis ($\rho_3 n$) is smooth and the new macrophage capacity influx term ($F_a a$) does not cause any trouble either. Like in Section 1.2, we would like to define an open domain Ω with negative lower bounds, so we could take initial values to be zero. When checking the modLDL uptake term ($\rho_1 P_l lm$, with P_l as in (3.2)), it shows that it is only smooth for l, a strictly positive. For $\epsilon a = -l$, the denominator of the uptake term equals zero. When taking l, a strictly positive, the partial derivatives of $P_l \cdot lm$ given in (3.10) are continuous and bounded for m, l, a bounded. The same reasoning can be used for the term expressing phagocytosis of AB's ($\rho_4 P_a am$ with P_a as in (3.2)).

$$\frac{\partial}{\partial l}[P_l lm] = m\frac{l^2 - 2\epsilon la}{(l+\epsilon a)^2}, \qquad \frac{\partial}{\partial m}[P_l lm] = \frac{l^2}{l+\epsilon a}, \qquad \frac{\partial}{\partial a}[P_l lm] = -\frac{l^2 \epsilon m}{(l+\epsilon a)^2} \tag{3.10}$$

There are no other constraints for the variables in order to have a well defined system. We have shown that there exists a unique solution to (3.9) in the domain $(l, m, n, a) \in (0, L) \times (-\delta, C) \times (-\delta, N) \times (0, A)$ with L, C, N, A, δ some strictly positive real numbers. Because of the fact that $P_l \to 0$ and $P_a \to 0$ for l and a tending to zero respectively, we can define $P_l = 0$ for $l = 0$ and $P_a = 0$ for $a = 0$. This way, we can take zero as closed lower bound for the domain of l and a.

An overview of the model parameters and their meaning is given in Table 3.2.

Table 3.2: Model parameters. M stands for molar concentration, d for days and V stands for volume.

	dimension	meaning
F_0	$M \cdot d^{-1}$	concentration change per day
F_m	d^{-1}	macrophage capacity influx per day caused by one unit modLDL
F_a	d^{-1}	macrophage capacity influx per day caused by one unit AB's
ρ_1	$d^{-1} \cdot M^{-1}$	modLDL uptake speed
ρ_2	$d^{-1} \cdot M^{-1}$	macrophage capacity influx speed per unit cytokines
ρ_3	d^{-1}	apoptosis speed
ρ_4	$d^{-1} \cdot M^{-1}$	phagocytosis rate per unit ingested AB's
ρ_5	d^{-1}	necrosis rate of one unit AB's
s	$[-]$	control parameter for T-cell feedback
ϵ	$[-]$	competition parameter for phagocytosis of AB's and modLDL
κ	VM^{-1}	plaque volume per molar concentration lipid

3.2 Fitting the apoptosis model to data

The model has been tested using the same data as discussed in Chapter 2. The difference between the early plaque growth model and the new apoptosis model only lies in the growth curve and thus in the calculated initiation times. The initiation rate given by (2.1) does not change, which means that the likelihood functions ℓ derived in Chapter 2 can still be used. In the new model, (3.9), the volume of a plaque consists of foam cells and necrotic core content so we compute a plaque volume as $V = \kappa(n + c)$, again using κ as a conversion parameter. All parameters are strictly positive and some parameters can be fixed according to [6]; F_0 is fixed to be $3.32 \cdot 10^{-8} M \cdot d^{-1}$ and parameter s from the T-cell feedback function is fixed at 10^{10}. In the same article, it is derived that $F_m \sim 10^{-2} \cdot s^{-1} \sim 10^{1} \cdot d^{-1}$. For the parameters that are not fixed, a search domain is defined in which the likelihood function should be maximized (or the -ln-likelihood should be minimized). Solving the system of equations numerically is done by a Fortran routine called DASSL, which can be found online for free[1] [11]. Minimizing the likelihood function (2.11) is done using a Fortran routine called Adaptive Simulated Annealing (ASA), which will be explained briefly before discussing the optimizations.

The underlying algorithm to ASA is Simulated Annealing (SA), an algorithm designed to find the global minimum for some function. In order to minimize a function f using SA, a starting point x_0 in the search domain is chosen. From a point x_k with $k \geq 0$ in the search domain, a new point x_{k+1} is constructed. This new point is accepted according some acceptance rule such that $f(x_k)$ converges to the optimal value for f as k grows. The way of generating a new solution from an old one depends on the solution space and the problem that is solved. A solution x_{k+1} is always accepted if $f(x_{k+1}) \leq f(x_k)$. If x_{k+1} is not an improvement compared to x_k, it can still be accepted with

[1] `http://cse.cs.ucsb.edu/software`

probability $\exp(-\Delta f/T(k))$. Here, $\Delta f = f(x_{k+1}) - f(x_k)$ and $T(k)$ is referred to as 'temperature'. The temperature decreases as k increases. This makes that solutions that are a degradation are accepted easily when computations just started and less easily when computations advance. By accepting 'bad' solutions, the risk of getting stuck in a local minimum instead of finding the global minimum is reduced. The decrease in temperature depends, like generating new solutions, on the problem. ASA is used to optimize a $D-$dimensional problem. Some parameters may be more sensitive to change than others and therefore, the model is re-initialized after a certain number of steps. More information about ASA can be found on the website of the author of the code[2]. The general simulated annealing algorithm is often used and information about it can be found in many books and online. In [5], both simulated annealing and adaptive simulated annealing are discussed.

There are different aspects to judging a solution. First of all, the likelihood of a solution should be good. While testing the model, it showed that the routine often gives a good likelihood but with a biological unlikely solution. The system has a lot of parameters and too many to produce one unique good fit, especially when using a small data set. In our tests, many different sets of parameter values return a good likelihood. The fact that our data set only contains plaque area's and no information about the formation of necrotic core also makes that there is no unique best fit. The optimization code is written such that ASA returns likelihood value 10^{30} if the new system cannot be solved with the selected parameters in the given search domain. The likelihood is therefore primarily used to determine whether the parameters that were found define a solvable system or not and secondly, to judge the likelihood of the solution. We find different types of behavior from the system and therefore, the resulting curves are judged on biological plausibility as well. Multiple fits were done, of which two scenario's that we thought to be biologically plausible are shown in Figure 3.2. The scenario's had an equal likelihood. Figure 3.3 shows single terms from each of the equations and parameters corresponding to these scenario's are listed in Table 3.3. The different scenario's are discussed in more detail below.

	sc. 1	sc. 2
ρ_1	$1.53 \cdot 10^{-2}$	$2.47 \cdot 10^{-2}$
ρ_2	$1.92 \cdot 10^{3}$	$3.09 \cdot 10^{2}$
ρ_3	$3.13 \cdot 10^{-3}$	$4.48 \cdot 10^{-2}$
ρ_4	$6.85 \cdot 10^{2}$	$2.05 \cdot 10^{3}$
ρ_5	$4.06 \cdot 10^{2}$	$1.28 \cdot 10^{1}$
F_m	$9.15 \cdot 10^{1}$	$3.87 \cdot 10^{2}$
F_a	$2.88 \cdot 10^{2}$	$1.31 \cdot 10^{-1}$
ϵ	$1.80 \cdot 10^{6}$	$2.24 \cdot 10^{6}$
κ	$2.90 \cdot 10^{5}$	$1.52 \cdot 10^{6}$

(a) Deterministic fit parameters.

F_0	$3.32 \cdot 10^{-8}$
s	10^{10}
τ	14

(b) Fixed parameters.

	sc. 1	sc. 2
α	0.08901	0.3931
λ_0	0.01338	0.01230

(c) Stochastic fit parameters.

Table 3.3: Parameter values for the scenario's shown in Figure 3.2 and Figure 3.3. Dimensions of the deterministic fit parameters are listed in Table 3.2

[2] `http://www.ingber.com/ASA`

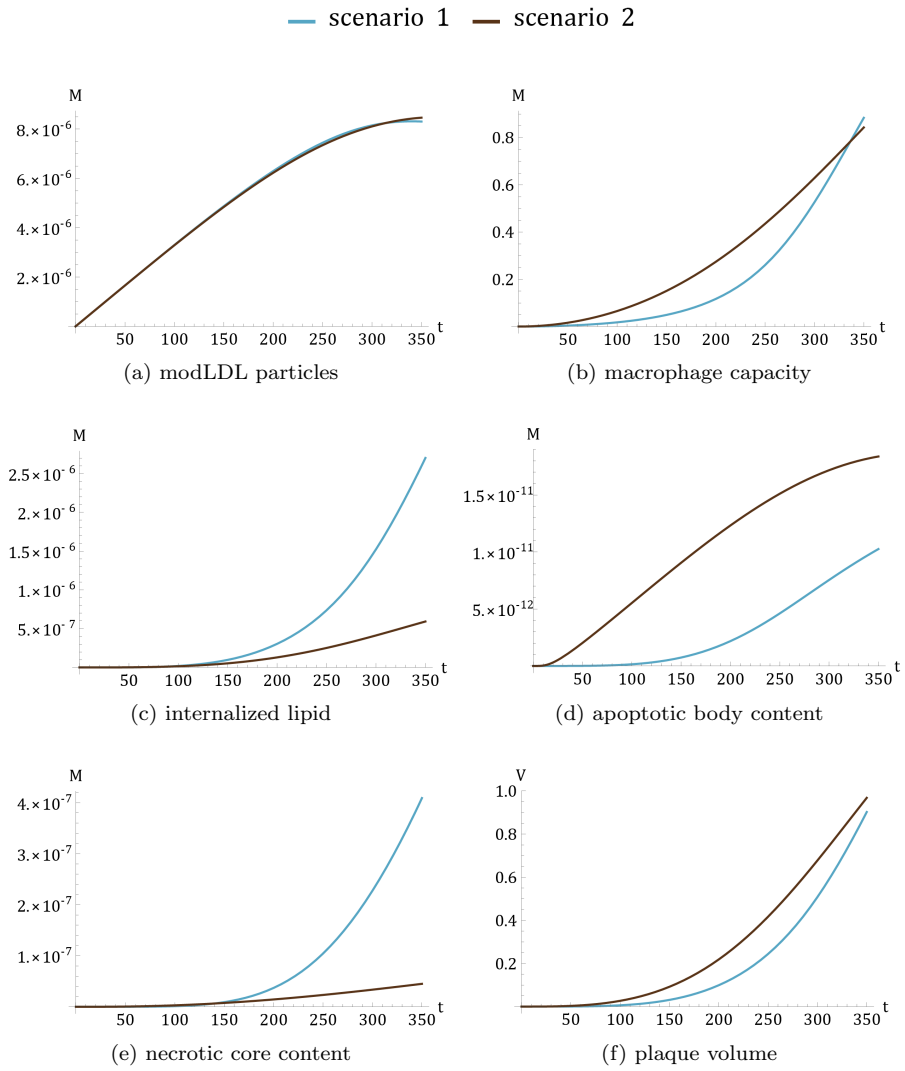

(a) modLDL particles (b) macrophage capacity

(c) internalized lipid (d) apoptotic body content

(e) necrotic core content (f) plaque volume

Figure 3.2: Two possible scenario's resulting from fitting the apoptosis model (3.9) to experimental data. The parameter values corresponding to the scenario's are listed in Table 3.3. Time t is in days, volume V is in mm^3.

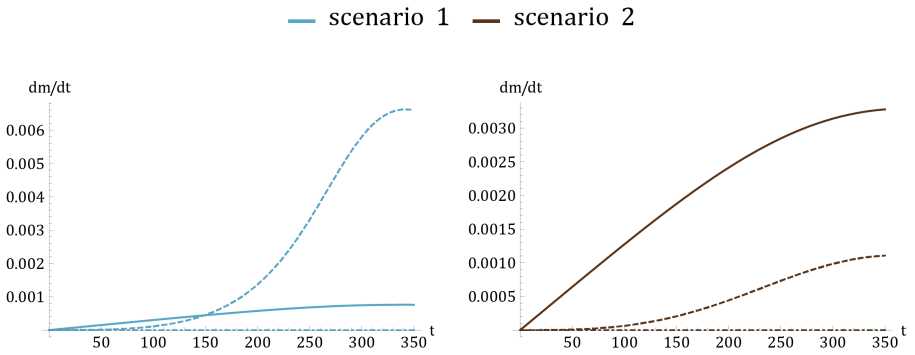

(a) Macrophage capacity recruitment. Solid: endothelial response. Dashed: T-cell feedback. Dotdashed: inflammation caused by apoptotic bodies.

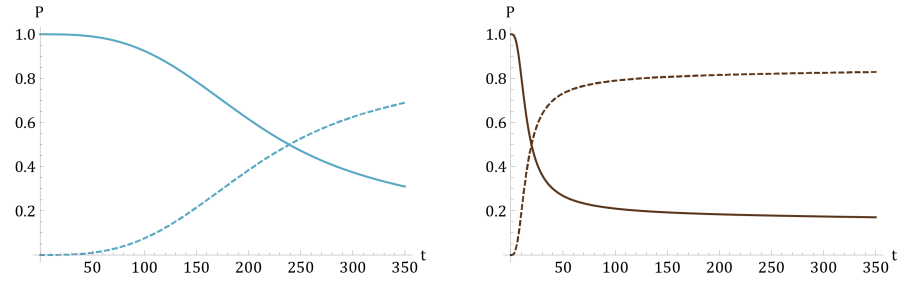

(b) Probabilities for a macrophage to take up modLDL or AB's. Solid: P_l. Dashed: P_a.

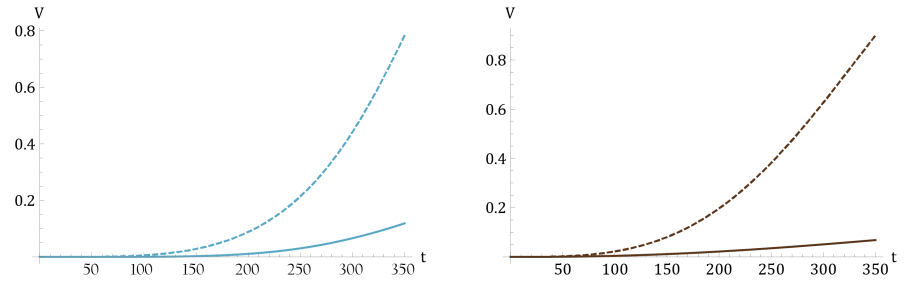

(c) Plaque components. Solid: necrotic core. Dashed: internalized lipid.

Figure 3.3: Separate components from each of the equations in the new model describing apoptosis. The parameter values corresponding to the scenario's are listed in Table 3.3. Time t is in days, volume V is in mm^3.

In the new model, there are three terms that express the recruitment of extra macrophage capacity; the endothelial response to modLDL, the T-cell feedback and the inflammatory effect of apoptotic bodies. The three separate terms are depicted in Figure 3.3a. In the first scenario, the largest part of the macrophage capacity influx is due to the T-cell feedback, while in the second scenario the endothelial response is the leading mechanism. The parameter values for ρ_2 for T-cell feedback and F_m for endothelial response as listed in Table 3.3 fit this observation; in the first scenario is $F_m < \rho_2$ and in the second scenario is $F_m > \rho_2$. The inflammation caused by apoptosis, expressed by the term $F_a a$, can be neglected compared to the other two recruitment mechanisms, which is a consequence of the apoptotic body content being small.

In Figure 3.2c, we see that the first scenario has a higher internalized lipid concentration than the second scenario. The ratio between the uptake parameter ρ_1 and the apoptosis rate ρ_3 explains this; in the first scenario is $\rho_1 > \rho_3$ while in the second scenario we found $\rho_1 < \rho_3$. The value for ρ_3 also influences the apoptotic body content, shown in Figure 3.2d. The apoptosis rate ρ_3 in the second scenario is large compared to the first scenario, resulting in a large apoptotic body content. In both solutions, the AB content is small, which is a result of ρ_4 and ρ_5 being large in comparison with ρ_3. More about this is discussed in Section 3.2.2. The difference in necrotic core content in the two scenario's, shown in Figure 3.2e, is a direct consequence of the difference in the values found for ρ_5.

The competition parameter ϵ does not have a clear meaning, as there is no information available about the correlation between phagocytosis and the uptake of modLDL. We defined the search domain for ϵ such that $\epsilon a \sim l$, so that the probabilities P_a and P_l do not take values one and zero. In this way, the uptake of modLDL and the phagocytosis of AB's are both modeled.

3.2.1 Comparing the initial growth model with the apoptosis model

The initial growth model (1.1) returned a rapidly growing function for the plaque volume. We expect that in reality the growth curve of a plaque flattens after some time, which we tried to model by incorporating apoptosis and subsequent necrosis. A comparison is made between a scenario of the early plaque growth model (1.1) from [6] and the apoptosis model (3.9) in Figure 3.4. The plots show that in the apoptosis model, the plaque growth is less explosive or even flattens after some time, as desired. To what extend the plaque volume curve flattens depends on what part of the apoptotic bodies is phagocytosed and removed from the plaque. As we mentioned before, we have no information about the necrotic core size and thus about the effectiveness of phagocytosis. We stress that the apoptosis scenario's depicted in Figure 3.4 are two possible solutions among many. The plots only show that it is possible to find solutions for the apoptosis model for which the plaque growth speed slows down after some time.

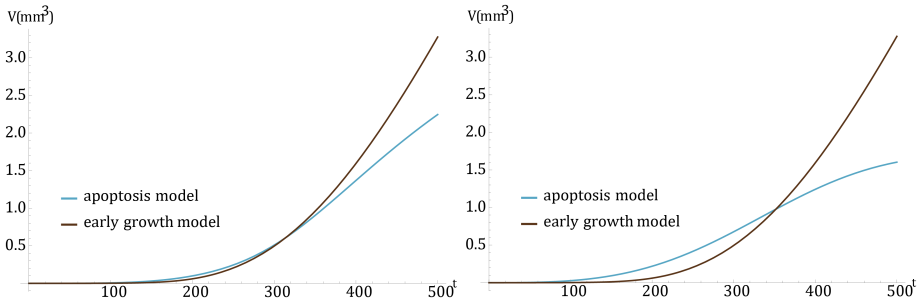

(a) scenario 1 (b) scenario 2

Figure 3.4: Plaque growth curves resulting from the early growth model (1.1) and the apoptosis model (3.9). The parameter values for the two scenario's are as listed in Table 3.3.

3.2.2 Time scales and quasi steady states

As mentioned before, the processes of phagocytosis and secondary necrosis are considerably faster than the other processes in our model. This means that in comparison to ρ_3 the parameters ρ_4 and ρ_5, which describe the rate of these fast processes, are large regardless of what time scale we use. In the time scale of plaque growth, the formation of apoptotic bodies and the almost immediate removal is barely noticeable. In other words, the concentration of apoptotic body content increases slowly but decreases rapidly. This makes that a adapts to the other, slow, variables quickly and we can therefore use a quasi steady state approximation (qssa) for a. By doing so, we can remove one variable. We find the quasi steady state for a (denoted by $\bar{a}(t)$) when setting the time derivative of a to be zero. From this, a dependence of a on the model parameters and variables follows:

$$\begin{aligned} &\frac{da}{dt} = 0 \\ &\qquad \Rightarrow \ \bar{a}(t) \ = \ \frac{\rho_3 n\epsilon - \rho_5 l + \sqrt{(\rho_3 n\epsilon - \rho_5 l)^2 + 4\rho_3 nl(\rho_4 \epsilon m + \rho_5 \epsilon)}}{2(\rho_4 \epsilon m + \rho_5 \epsilon)}. \end{aligned} \tag{3.11}$$

We verified that this approach works for a simple linear example, which is demonstrated in the Appendix. We also refer to [2, p. 267] for an example of the usage of the qssa. For the two scenario's, we computed $a(t)$ numerically and the quasi steady state approximation $\bar{a}(t)$ as given in (3.11). In Figure 3.5, we depict the absolute relative error $\eta = |a(t) - \bar{a}(t)|/a(t)$ between the two functions. The figure shows clearly that, after a first short initialization period, the error becomes small.

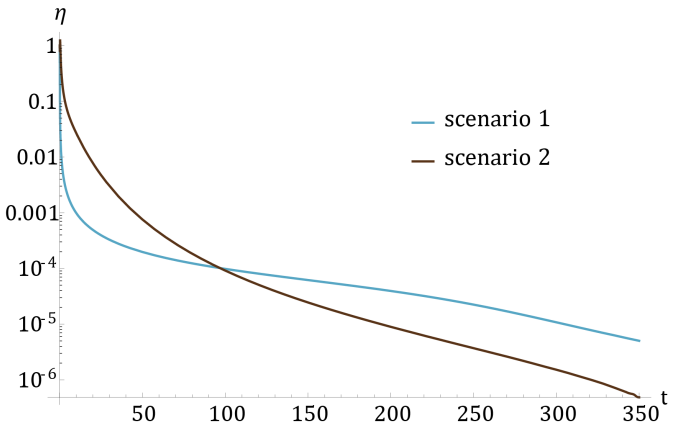

Figure 3.5: The absolute error $\eta = |a(t) - \bar{a}(t)|/a(t)$ between the numerical solution $a(t)$ of (3.9) and the quasi steady state approximation $\bar{a}(t)$, as given in (3.11). The two scenario's are as listed in Table 3.3 and time t is in days.

Next, we numerically compute the solution to the subsystem (3.9a), (3.9b), (3.9c), (3.9e) substituting the qssa $\bar{a}(t)$. We use the parameter values from the scenario's listed in Table 3.3. Again, we compute the absolute relative error between the solutions $l(t), m(t), n(t), c(t)$ of the complete system and the solutions $\bar{l}(t), \bar{m}(t), \bar{n}(t), \bar{c}(t)$ of the subsystem using $\bar{a}(t)$. The results are shown in Figure 3.6.

Summary. We conclude that it is possible to find the expected biological behavior from our new apoptosis model. However, the amount of parameters is too high, so in practice the model can be only used to compute possible scenario's. The time scale differences in the biological processes can be used to eliminate one variable from the system, namely the apoptotic body content a. This results in a system with four differential equations for modLDL (l), macrophage capacity (m), internalized lipid (n) and necrotic core content (c). For apoptotic body content we can use the quasi steady state approximation $\bar{a}(t)$. Would there be more known about the parameter values that appear in the expression (3.11) for the qssa, the expression $\bar{a}$ could be simplified and we would probably be able to draw conclusions about the asymptotic behavior of a.

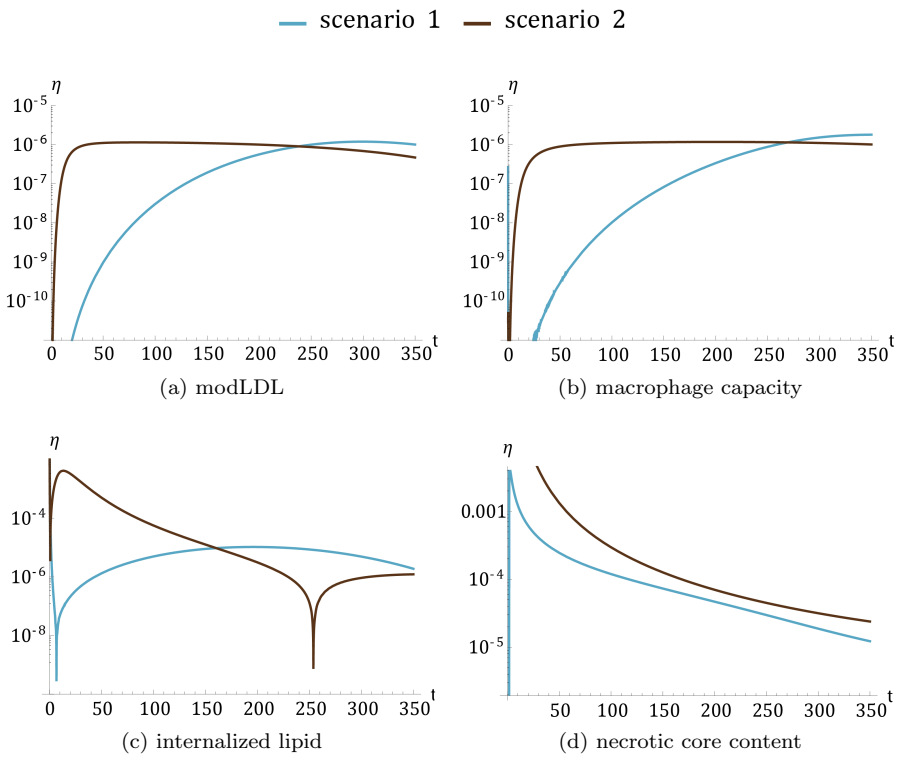

(a) modLDL (b) macrophage capacity

(c) internalized lipid (d) necrotic core content

Figure 3.6: The absolute relative error η between the solution of the complete set of equations and the solution to the subset of equations $(\bar{l}, \bar{m}, \bar{n}, \bar{c})$ using the quasi steady state approximation for apoptotic body content $\bar{a}$. Time t is in days.

4 Overlapping plaques

In addition to the data that was modeled in the previous chapter, there are new data available [8]. Again, mice have been irradiated with X-rays, but this time to a dose of 0, 0.3 or 6 Gray. In total, 27 mice were (sham) irradiated at the age of 60 days and sacrificed at the age of 360 days. The number of plaques and plaque areas were evaluated in the descending aorta and the aortic arch. This data was fitted using the same procedure as discussed in Chapter 2 using the initial set of differential equation for early plaque growth (1.1). Results from these fits returned large values for the expected plaque area compared to the measured values which was a reason to look into the data more carefully.

A striking feature of the data can be observed in Figure 4.1; there is a large spread in plaque sizes. The data showed that for the sham treated mice, the largest and second largest plaques are almost equal in size, but they differ a factor 1.5× with the third largest plaque. For the 0.3 Gy dose group, the largest plaque in the descending aorta is a factor 1.5× larger than the second largest plaque. For the 6.0 Gy dose group, this difference is even a factor 2×. Measured values for the descending aorta are shown in Figure 4.1. Plaques in the aortic arches are considerably larger than in the descending aorta. For the 0.3 Gy dose group, the difference in largest and second largest plaque is also a factor 1.5×. For the other dose groups, plaque sizes are distributed more evenly but still there is a large size difference between small and large plaques.

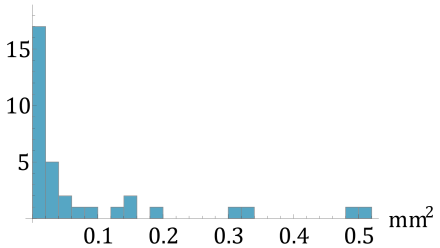

(a) 0 Gy

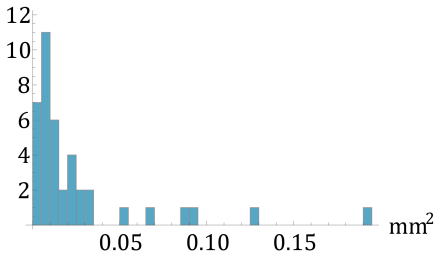

(b) 0.3 Gy

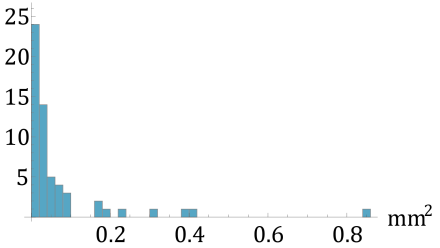

(c) 6 Gy

Figure 4.1: Histograms of measured plaque areas per dose group. There were 9 mice in each dose group. Plaques are measured in the descending aorta. Note the difference scales on the axes.

In a model with a universal growth curve for each plaque, the plaque growth rate should be large enough to reach the largest plaque size within 360 days, the lifespan of the mice. The largest plaque in a dose group will be formed at an early age. The smaller plaques have their expected initiation time many days later due to the large difference in size. This makes that the expected initiation times of the smaller plaques will be modeled to lie in the last days or weeks before the mice were sacrificed. We have shown before however that radiation has an increasing

effect on the initiation rate of plaques and thus that more plaques are expected to be formed in the time window between irradiation and the following two weeks. The mice were irradiated at 60 days, so the result of most of the plaques being formed in the last days before the sacrifice does not seem plausible. From all this, it was deduced that the largest plaques are probably multiple plaques that merged together. The possibility of overlapping plaques was later confirmed by researchers of the Erasmus Medical Center.

Until now, fitting was done by computing expected initiation times for every plaque. This is not possible when modeling overlapping plaques. We do not know whether a measured plaque actually is built up from multiple plaques and if so, how many. Instead of considering individual plaques, we decided to model the covered area in a piece of the artery that is cut open to form a rectangle, see Figure 4.2. In what follows, we use notations as defined below.

Definition 4.1. Let the size of the rectangular artery subsection be denoted by F. The size of the area in F that is covered by plaque is denoted by ψ. We denote for a point x that lies in covered area $x \in \psi$, meaning that we use ψ as a measure for the covered area but also to denote the set of covered points.

We derive an equation for the expected coverage $\psi(t)$. In an artery, it is possible for a plaque to be initiated outside of F but within distance of the plaque radius of F. Then, part of the plaque is in fact in F. This is most easily modeled using periodic boundary conditions. Cutting an artery might split up one plaque, which motivates us to use periodic boundary conditions in the other direction as well. Boundary conditions are depicted in Figure 4.2. As a start, we model plaques as disks that all have the same size upon initiation. Later, the growth of plaques is incorporated.

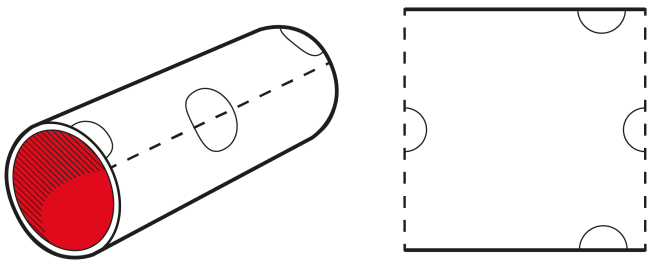

Figure 4.2: Cutting of an artery. We use periodic boundary conditions in our simulations and in our derivation of the differential equation describing coverage.

4.1 Plaques with a fixed size

As a start, the plaques are modeled as randomly placed disks that all have the same circular area a_0 upon initiation and that are initiated sequentially. In this model, we allow the disks that represent the plaques to overlap but their center, which we refer to as initiation point, should lie in area still uncovered by plaques, i.e. not in ψ. In later stages of atherosclerosis, it is possible for plaques to form on top of other plaques but this is not investigated here. Further assumptions

on the spatial distribution are not made meaning that we model the coverage as if it was uniformly spread over F and ψ will describe the average coverage in a large sample of arteries. An equation for the expected increase in coverage $d\psi$ in a small time interval $[t, t + dt]$ caused by random initiation of plaques is deduced.

Plaques are formed with a certain net initiation rate $\lambda(t)$, as was described in Chapter 2. For now, we do not incorporate radiation in this rate. By our requirement that the initiation points of plaques do not lie in ψ, the number of plaques that arise in a short time interval gets smaller as the covered part of the artery gets larger, that is as $\psi(t)$ grows towards F. The net initiation rate, or successful initiation rate, is thus dependent on the total coverage. It is however not dependent on the spatial characteristics of the artery, since we aim to describe the average behavior for arteries in a large sample. We model the net initiation rate $\lambda(t)$ as the product of some baseline event rate λ_0, which is the initiation rate per unit free area, and the probability for a plaque to have its initiation point not in ψ. This probability is proportional to the free space $F - \psi$. With $\lambda(t)$ like this, the rate with which plaques are successfully initiated approaches zero as ψ approaches F, as desired.

$$\lambda(t) = \lambda_0 \cdot \left(\frac{F - \psi(t)}{F} \right) \tag{4.1}$$

In a small time interval $[t, t + dt]$ of length dt, the expected number of successful initiations equals $\lambda(t)dt$. The new plaques will contribute to ψ, but how much they contribute depends on the size of the part that is already covered. As ψ increases towards F, the probability for a new plaque to partly overlap with existing plaques gets larger and the expected contribution of this single plaque to ψ gets smaller. If there were no restrictions on the initiation point, the expected contribution to ψ of a plaque $\mathcal{P}$, initiated at time t and with fixed size a_0 would be computed as below.

$$\int_{\mathcal{P}} P(x \text{ uncovered}) dx = \int_{\mathcal{P}} \left(\frac{F - \psi(t)}{F} \right) dx = a_0 \cdot \left(\frac{F - \psi(t)}{F} \right) \tag{4.2}$$

However, we require the initiation point of a plaque to lie in free area. We should therefore take into consideration that for a point x in a disk $\mathcal{P}$ with its center c in free area $F - \psi$, the probability to lie in free area as well is larger then when the center c of the disk would have been randomly placed in F. This is in Figure 4.3 and in short, means that

$$P(x \notin \psi \mid x \in \mathcal{P}) < P(x \notin \psi \mid x \in \mathcal{P} \textbf{ and } c \notin \psi). \tag{4.3}$$

The true expected contribution to the coverage ψ equals $\int_{\mathcal{P}} P(x \notin \psi | x \in \mathcal{P} \text{ and } c \notin \psi) dx$, which is larger than the expression in (4.2). We were unable to find an analytical expression for the right hand side probability in (4.3) ourselves nor did we find an expression in literature. In order to model the probability, we heuristically add a parameter $\nu \in [0, 1]$; we assume that $P(x \notin \psi | x \in \mathcal{P} \text{ and } c \notin \psi)$ equals $((F - \psi)/F)^\nu$. Combining the above gives us the average expected increase in ψ in a time interval $[t, t + dt]$ caused by new plaques, as given below. The resulting differential equation

$$\frac{d\psi}{dt} = \lambda_0 \left(\frac{F - \psi}{F} \right) \cdot a_0 \left(\frac{F - \psi}{F} \right)^\nu \tag{4.4}$$

is solvable with solution

$$\psi(t) = F - F\left(1 + \frac{a_0 \cdot \lambda_0 \cdot \nu \cdot t}{F}\right)^{-\frac{1}{\nu}}. \tag{4.5}$$

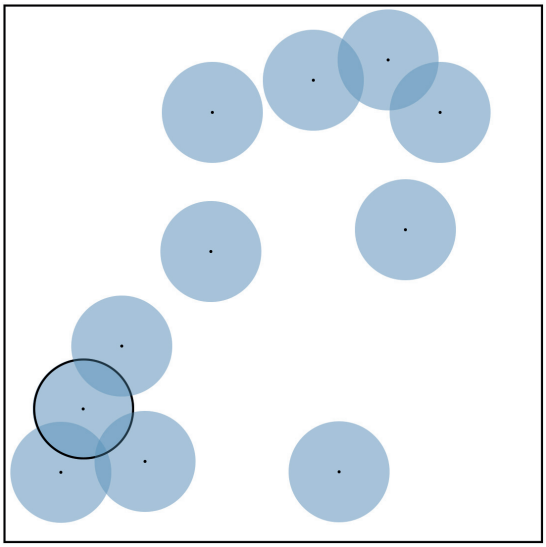

Figure 4.3: Plaques may overlap, but we assumed that their initiation points lie in uncovered area. The contribution to ψ of the last initiated plaque (marked) depends on the earlier formed plaques. We compute for each (infinitesimal small) point on the newest plaque the probability to lie in area that has not yet been covered by previously formed plaques, given that the initiation point of the newly formed plaque lies in uncovered area.

We did not succeed in finding an exact, analytical value for ν, which may depend on plaque size a_0. We used numerical simulations in which F was taken to be 1×1 and divided it in a grid of $10^3 \times 10^3 = N$ points. During the simulation, grid points are labeled to belong to ψ or not in order to determine the coverage, which is computed as the ratio between grid points belonging to ψ, N_ψ, and the total number of grid points N. At the start of the simulation, ψ is set to be empty. We took λ_0 equal $1/dt$ in order to simplify calculations; the rate λ_0 is set to one initiation attempt per time step $dt = 1$. One attempt in the simulation is just the selection of a random grid point g. Then, it is determined whether this point belongs to ψ or not. If $g \notin \psi$ the attempt is successful, meaning that this point is stored as an initiation point and all grid points surrounding g within the plaque radius are set to belong to ψ. If $g \in \psi$, no new initiation occurs so no new points are set to belong to ψ. After every attempt, the ratio N_ψ/N is stored.

We should make a remark about the choices we made in our simulations. An initiation attempt (selecting a random point g) is independent of the previous attempts and whether they were successful or not. This means that the attempts behave as a Poisson process with event rate λ_0 and the probability to have k initiations in a short time step $\Delta t \ll dt$ is as follows:

$$P(k \text{ initiations in } \Delta t) = \frac{(\lambda_0 \Delta t)^k}{k!} e^{-\lambda_0 \Delta t}. \tag{4.6}$$

The case of $k > 1$ is negligible since powers of $\lambda_0 \Delta t$ are small. With λ_0 chosen equal to 1, the probability to have one initiation attempt in Δt equals approximately Δt which leads to an average of one initiation attempt per time

step $dt = 1$. We implemented this average by forcing the simulation to choose one g per time step dt, even though more precise would be to divide dt into smaller time steps Δt and perform an attempt (meaning selecting a g randomly) with probability Δt each time step. The probability of having no attempt at all, meaning that no point g is selected and the simulation continues to the next time step, is then $1 - \Delta t$.

The simulations are performed 250 times for plaque radii $0.005, 0.01, 0.05$ and 0.1 respectively. Even for the smallest radius one plaque covers multiple grid points, so the chosen resolution of the grid is assumed to be sufficiently fine. We fitted the equation in two differen ways. For the first procedure, we computed the average covered area at every time step from all 250 simulations. We fitted this mean curve to (4.5) using the standard findfit function in Mathematica, which resulted in an optimal value for the parameter ν, denoted by $\widetilde{\nu}$. This is done because the differential equation (4.4) is derived using averaging and expected values. The results of these fits are listed in Table 4.1. As an alternative, to find out how well the solution to the differential equation works for separate simulations, we fitted the 250 simulated curves for covered area separately to (4.5). Again, we used the standard findfit function in Mathematica. The mean of the results of these separate fits, denoted by $\langle \nu \rangle$ and the standard deviation are also listed in Table 4.1. Figure 4.4 shows the curves of (4.5) using $\widetilde{\nu}$ as listed in Table 4.1 and the curve for ψ that follows from averaging the simulations.

The values for $\widetilde{\nu}$ and $\langle \nu \rangle$ are similar for all plaque sizes. The spread in results in the separate fits is larger for larger plaques, which can be explained as follows. For relatively large plaques, ψ grows rapidly at the start of the experiment, causing a fast decrease in the net initiation rate $\lambda(t)$. In a short amount of time steps, the difference in spatial configuration of ψ can get large for different runs and thus, the separately fitted values for ν will differ considerably. By taking more runs, the standard deviation can be reduced. We started with 100 simulations and later added new runs to get 250 simulations. From the values in Table 4.1, it seems reasonable to fix ν at the value 0.48.

The difference between the smallest and the largest a_0 that we used is a factor 400, which is quite large and from the simulations, we found no clear dependence on the disk size. This can be explained by the fact that we used similarly shaped plaques and the fact that we used periodic boundary conditions. The main difference between the simulations is the scaling of the system. The fact that, especially for small plaque sizes, the standard deviation for separate fits is small and that $\widetilde{\nu}$ is similar to $\langle \nu \rangle$ means that (4.5) is a good description.

Table 4.1: $\widetilde{\nu}$: results of fitting the mean of 250 simulations to (4.5). $\langle\nu\rangle$: mean of the results for ν for 250 separate fits to (4.5). SD: standard deviation of $\langle\nu\rangle$.

radius	0.1	0.05	0.01	0.005
$\widetilde{\nu}$	0.482713	0.484303	0.471230	0.473278
$\langle\nu\rangle$	0.476411	0.483020	0.471186	0.473268
SD	0.09331	0.03941	0.009671	0.004515

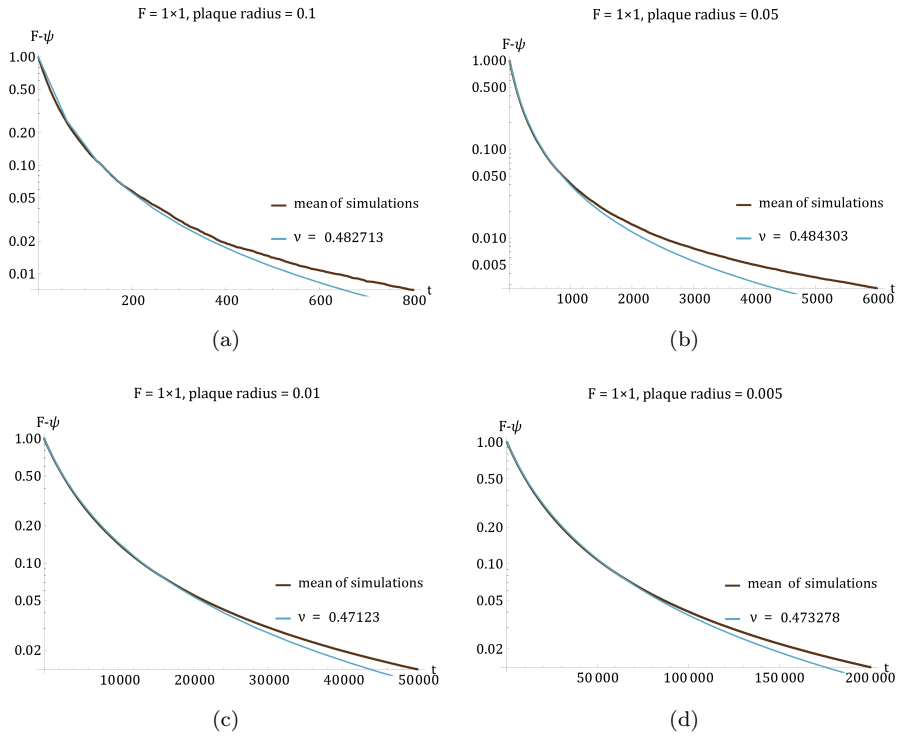

Figure 4.4: Plots of the uncovered fraction of F. Notice the logarithmic scale for $F - \psi$ and the different time scales on the different horizontal axes. (4.5) is plotted using $\widetilde{\nu}$. The simulations are averaged and the mean covered area from 250 simulations is shown.

4.2 Growing plaques

The next step is to develop a model for growing plaques. We use the same notation covered and total area as in the previous section. Again, we assume that plaques originate in area that is still uncovered so the net initiation rate $\lambda(t)$ is equal to (4.1). We assume that all plaques have the same growth curve $a(t)$ with $a(0) = a_0$ and that they are circular. Note that $a(t)$ describes plaque area and has nothing to do with the equation for apoptotic body content in Chapter 3. In reality, the growth of a plaque depends on the age of the test animal, the plaque location and the amount of plaque that has already formed in the artery. We also suspect that plaques that overlap develop differently than plaques that do not, but we ignore this in our model and we describe the plaques as growing disks. In a number of steps, we deduce the expected increase $d\psi$ in coverage in a small time interval $[t, t + dt]$ caused by the growth of plaques that were initiated before time t and the formation of new plaques. Denote initiation times by t_i and let the formation of plaques in the model begin at time $t = 0$.

Fix the current time at t. For one plaque that was initiated at $t_i \geq 0$, the growth in $[t, t + dt]$ *without taking overlap into account* is given by the following:

$$a(t + dt - t_i) - a(t - t_i). \tag{4.7}$$

Now consider a historical, short time interval $[s, s + ds]$ with $s + ds \leq t$. The expected number of initiations in this time interval can be computed using the initiation rate $\lambda(s)$ as defined in (4.1):

$$\lambda_0 \cdot \left(\frac{F - \psi(s)}{F}\right) \cdot ds. \tag{4.8}$$

When combining (4.7) - (4.8), the expected increase in ψ in the time interval $[t, t + dt]$ that is caused by plaques that were initiated around s but *without taking overlap into account* can be computed. For infinitesimally small dt, the time derivative of the growth curve a in time $t - s$ can be introduced, denoted by a dot.

$$\begin{aligned} &\overbrace{\lambda_0 \cdot \left(\frac{F - \psi(s)}{F}\right) \cdot ds}^{\text{expected number of formed plaques}} \quad \cdot \overbrace{[a(t + dt - s) - a(t - s)]}^{\text{growth per plaque}} \\ &\qquad = \lambda_0 \cdot \left(\frac{F - \psi(s)}{F}\right) \cdot ds \cdot \dot{a}(t - s)dt \end{aligned} \tag{4.9}$$

All plaques that were formed up to time t will grow, so we have to account for all initiation times up to t. This is done by integrating over s, which results in a term describing the expected growth of all plaques that were initiated up to time t, but still *without taking overlap into account*:

$$\int_0^t \lambda_0 \cdot \left(\frac{F - \psi(s)}{F}\right) \cdot \dot{a}(t - s)dt \cdot ds. \tag{4.10}$$

The actual expected increase in ψ in the interval $[t, t + dt]$ turns out to be smaller than (4.10). This is because in the expression (4.10), we still did not deal with

the random overlap. As time t gets larger only a fraction of the integral will contribute, so a correction factor dependent on t must be added. This factor is modeled in the same fashion as the correction factor in the previous section. The expected difference in ψ caused by the growth of existing plaques, $d\psi_{hist}$ is given by

$$d\psi_{hist} = \left(\frac{F-\psi(t)}{F}\right)^{\mu} \cdot \int_0^t \lambda_0 \cdot \left(\frac{F-\psi(s)}{F}\right) \cdot \dot{a}(t-s)dt \cdot ds. \tag{4.11}$$

The expected growth in ψ caused by newly initiated plaques in $[t, t+dt]$ with fixed initial size a_0, $d\psi_{new}$ is modeled by (4.4) as explained in the previous section:

$$d\psi_{new} = \lambda_0 \left(\frac{F-\psi(t)}{F}\right) dt \cdot a_0 \left(\frac{F-\psi(t)}{F}\right)^{\nu}. \tag{4.12}$$

The two equations (4.11) and (4.12) are combined to find, after taking the limit of $dt \to 0$, an overall differential equation that describes the total expected increase in ψ:

$$\begin{aligned} \frac{d\psi}{dt} &= \lambda_0 \cdot a_0 \cdot \left(\frac{F-\psi}{F}\right)^{\nu+1} \\ &\quad + \lambda_0 \left(\frac{F-\psi}{F}\right)^{\mu} \cdot \int_0^t \left(\frac{F-\psi(s)}{F}\right) \cdot \dot{a}(t-s)ds. \end{aligned} \tag{4.13}$$

4.2.1 Using simulated annealing to find parameter values

The values for μ and ν are unknown, as it was for ν in the previous section. Again, we performed computer simulations in order to find the best fitting parameters. The simulations were set up like the simulations for plaques with a fixed size; an area $F = 1 \times 1$ was divided into a grid, but this time the grid was 2000×2000 in order to be able to start with small values for a_0. Initially, all grid points belong to uncovered area. We set $\lambda_0 = 1$, meaning that in every time step dt we perform one initiation attempt. As before, we pick one grid point g randomly during each time interval $[t, t+dt]$. The same remark as in the previous section can be made about the simulations. Actually, the attempts behave as a Poisson process. Taking $\lambda_0 = 1/dt = 1$ leads to on average one attempt per time step dt and this average is what we implemented in our simulations. Whether a plaque is in fact initiated depends on the position of g; if it lies in uncovered area it serves as a new initiation point and the initiation attempt resulted in a new plaque. If g is chosen and if this grid point does not belong to ψ, an area of size a_0 around g is set to belong to ψ. For every plaque, the initiation point g and its initiation time t_i are stored. After this, growth of existing plaques is computed. This is done by computing the radius of an existing plaque at the current time t, $r = \sqrt{a(t-t_i)/\pi}$, and setting all grid points within a distance r from the initiation point g to belong to ψ. Different growth curves $a(t)$ are used, see (4.15) and (4.16). After each time step, the coverage N_ψ/N is stored. This results in a solution vector ψ_s containing $\psi_s(t)$ at times $t = 0, 1, 2, \ldots$.

Equation (4.13) cannot be solved analytically, so the standard Mathematica findfit function cannot be used. The equation is, however, numerically solvable using the Fortran routine DASSL [11]. This routine computes values of ψ at

times t_k that are determined by the routine itself. It is possible to define a maximum step size. We denote ψ_d for the solution vector containing $\psi(t_k)$ of DASSL. The maximum time step size is set to be 0.1 and the integral (4.10) until time t_k is computed as a discrete sum $\sum_{j=1}^{k}(t_j - t_{j-1}) \cdot (1 - \psi(t_j)) \cdot \dot{a}(t - t_j)$, since $F = 1$. This sum is used to find $\psi_d(t_{k+1})$ and since the maximal time step is limited, it will be a reasonable approximation for the integral.

We have used a simulated annealing (SA) routine to minimize the relative absolute error η per simulation time step between the simulated curve ψ_s and solutions by DASSL ψ_d, resulting in the best fitting parameter values for μ and ν. For more general information about simulated annealing, we refer to Section 3.2. In the SA routine, the simulation vector ψ_s and initial values for the parameters (μ_0, ν_0) are given as input. Also, a lower and upper bound for the parameters is given $(\mu_{\min}, \mu_{\max}, \nu_{\min}, \nu_{\max})$ and a maximum number of simulated annealing steps $c_{\max}$. Furthermore, the starting temperature T is given as input. One SA step consists of first picking new parameters in the search domain randomly. We have implemented this by picking two uniformly distributed random numbers $p, r \in [0, 1]$. If $p < 0.5$, the next value for μ, μ_c is computed according to $\mu_c = \mu_{c-1} - r \cdot (\mu_{c-1} - \mu_{\min})$. If $p \geq 0.5$, we compute $\mu_c = \mu_{c-1} + r \cdot (\mu_{\max} - \mu_{c-1})$. The same is done for ν. By picking new parameters in this way, the value to which the parameters converge is solely defined by the quality of the solution given these parameter values and not by how the parameters are chosen from the search domain. Using DASSL, the solution to our differential equation (4.13) with these new parameter values is computed. Next, the absolute relative error η_c between the simulation and the DASSL solution is computed.

The DASSL solution ψ_d is given on times t_k, while the simulated curve is given on time $t = 0, 1, 2, \ldots$ so to compute the relative absolute error, linear interpolation is used to find the DASSL solution $\bar{\psi}_d$ at times $t = 0, 1, 2, \ldots$. Now, the relative absolute error can be computed:

$$\eta_c = \frac{1}{t_{end}} \sum_{t=1}^{t_{end}} \frac{|\bar{\psi}_d(t) - \psi_s(t)|}{\psi_s(t)}. \tag{4.14}$$

If the error with new parameters (η_c) is smaller than the error with the previous parameters (η_{c-1}), the new parameters are adopted. If on the contrary the new parameters decrease the quality of the fit, we pick a random number $p \in [0, 1]$ and if $p < \exp[-(\eta_c - \eta_{c-1})/T]$, we accept the new parameters even though it is a degradation. If they are rejected, we set $\mu_c = \mu_{c-1}, \nu_c = \nu_{c-1}$. The temperature is decreased at each step by multiplying with a factor smaller than one. This multiplication factor and the initial temperature are dependent on the problem.

4.2.2 Results from fitting

We use growth curves $a(t)$ that are given in (4.15). We chose these strictly increasing curves arbitrarily such that they stay below the order 10^{-1} at least until $t = 300$, as we took $F = 1 \times 1$.

$$a(t) = 10^{-5} + 10^{-3}t \tag{4.15a}$$

$$a(t) = 10^{-5}(1 + t^2) \tag{4.15b}$$

Again, we did 250 simulations and started by computing the average of all these curves. The mean growth curve of the simulations is fitted to the differential equation (4.13). The search domain for μ, ν is set to $[0,1] \times [0,1]$ and the temperature multiplication factor depends on the growth scenario. For linear growth we use factor 0.9999 and for quadratic growth 0.99975. We pick start values at $T_0 = 1.0$, $\nu_0 = 0.5$ and $\mu_0 = 0.5$ and we set the number of simulated annealing steps for linear growth to be 125.000 and for quadratic growth 50.000. These initializations are all based on some first trial runs. During the fitting, we kept track of the parameter values and corresponding η at each simulated annealing step.

The values that were found for both parameters are listed in Table 4.2 and denoted by $\widetilde{\mu}$ and $\widetilde{\nu}$. For linearly growing plaques, the optimal curve resulting from the fit is depicted in Figure 4.5 together with the mean coverage of 250 simulations. The plots also show the values for μ and ν per simulated annealing step. We see that the value for μ converges but the value for ν does not. The error η as a function of μ and ν is also shown. From these plots, we conclude that ν, in this setting, has no influence on the quality of the fits. For the quadratic growth curve, similar results hold (not shown). From the fitting results, we can also conclude that for different growth curves $a(t)$, different optimal parameter values hold. Again as a next step, we fit the DASSL solution of our differential equation to every simulation separately for each of the growth curves in (4.15). The means of the optimal parameter values that were found, denoted by $\langle\mu\rangle, \langle\nu\rangle$, and the standard deviations are listed in Table 4.2. They show clearly that the standard deviation for the values of ν is large, in contrast to the values of μ and that indeed, ν has no optimal value in this setting.

The fact that the parameter ν, which appears in the term describing the increase in covered area caused by newly initiated plaques, seems to have no influence on the error between simulations and (4.13) might be a consequence of a_0 being small in comparison to the growth of already existing plaques. Even though in real life plaques have no volume when they are initiated and a_0 should therefore be modeled as a point mass, we perform simulations using linear and quadratic growth but with a larger starting volume a_0. We perform simulations with the following two growth curves.

$$a(t) = 10^{-2} + 10^{-3}t \tag{4.16a}$$

$$a(t) = 10^{-2} + 10^{-5}t^2 \tag{4.16b}$$

The input for the simulated annealing routine is almost the same as in the previous runs for plaques with a smaller a_0. For linearly growing plaques, we perform again 125.000 simulated annealing steps but the temperature T is multiplied by 0.9998. For quadratically growing plaques, we perform 75.000 simulated annealing steps and multiply the temperature T by 0.99975. The initial temperature is taken to be 1 for both growth curves and for both growth curves, we use $\mu_0 = \nu_0 = 0.5$.

Again, as a first step the mean of 250 simulations is computed and fitted to (4.13). The resulting $\widetilde{\mu}, \widetilde{\nu}$ are listed in Table 4.3. Even though linear and quadratic growth showed similar results, the effect of the parameters was most noticeable in the figures for quadratically growing plaques, which are shown in Figure 4.6. The parameters per simulated annealing step show that both μ and ν converge to an optimal value $\widetilde{\mu}$ and $\widetilde{\nu}$ now. Especially the dependence of η on

both parameters in the last plot in Figure 4.6 shows that ν has some influence on the quality of the fit and that there is a correlation between μ and ν. As a next step again, the fitting is done for every simulation separately. The mean of these fitting results are listed in Table 4.3, as well as the corresponding standard deviations. The standard deviations for ν are still large in comparison to that of μ. This is probably a result of the large differences between configurations in the separate simulations.

Summary. We conclude that for the first set of simulations using fixed plaque sizes, the coverage equation $\psi(t)$ that was derived (4.5) is a good fit. The quality of the separate fits decrease as the plaques get bigger in comparison to the artery subsection F. For growing plaques, we conclude the following. From the first set of simulation using growth curves with a small initial size a_0, we conclude that optimal parameter values for μ differ for the different growth curves. From the simulations using growth curves with a larger initial size a_0, we conclude that there is a correlation between μ and ν. The correlation is strong when the history term and the new initiation term from (4.11)-(4.12) both influence the coverage of F. For the fits using a small initial plaque size, we conclude that ν has no influence on the quality because of a_0 being small. For the problem of overlapping plaques, this means that ν will play no part since $a_0 \to 0$. Separate fits for growing plaques do not work as well as the fits for fixed plaque sizes. However, we eventually want to fit the coverage equation (4.13) to experimental data. In the data sets, arteries are never fully covered. The quality of the separate fits to simulations will probably increase if the simulations are ended well before F is fully covered. In future research, we can take a plaque growth curve $a(t)$ following from the growth model presented in Chapter 3. Further discussion about our simulations and fitting results is presented in Chapter 5

Table 4.2: Fitting results of the two different growth curves (4.15) to the differential equation given in (4.13). $\widetilde{\cdot}$ are the optimal parameters found when fitting the mean coverage of 250 simulations. $\langle\cdot\rangle$ are the means of the optimal parameter values for 250 separate fits. $\mathrm{SD}_{\langle\cdot\rangle}$ are the corresponding standard deviations for the separate fits.

	linear	quadratic
$\widetilde{\mu}$	0.7700	0.9165
$\widetilde{\nu}$	0.1068	0.9685
$\langle\mu\rangle$	0.8177	0.9075
$\mathrm{SD}_{\langle\mu\rangle}$	0.09779	0.07728
$\langle\nu\rangle$	0.4935	0.7863
$\mathrm{SD}_{\langle\nu\rangle}$	0.3433	0.3313

Table 4.3: Fitting results of the two different growth curves (4.16) to the differential equation given in (4.13). $\widetilde{\cdot}$ are the optimal parameters found when fitting the mean coverage of 250 simulations. $\langle\cdot\rangle$ are the mean values of the optimal parameters for 250 separate fits. $\mathrm{SD}_{\langle\cdot\rangle}$ are the corresponding standard deviations from the separate fits.

	linear	quadratic
$\widetilde{\mu}$	0.7474	0.7873
$\widetilde{\nu}$	0.07284	0.3532
$\langle\mu\rangle$	0.7295	0.8264
$\mathrm{SD}_{\langle\mu\rangle}$	0.07790	0.06177
$\langle\nu\rangle$	0.3255	0.3554
$\mathrm{SD}_{\langle\nu\rangle}$	0.4178	0.3605

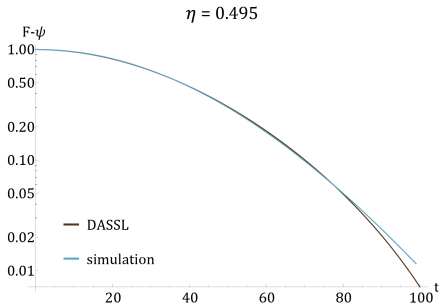

(a) Mean coverage of 250 simulations compared to the optimal curve resulting from the simulated annealing routine

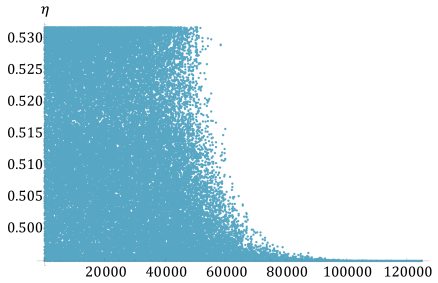

(b) Absolute relative error η per SA step. One run consisted of 125.000 steps.

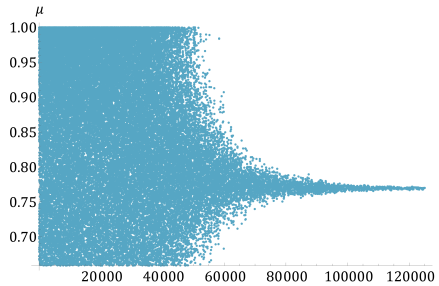

(c) Values for μ per SA step. One run consisted of 125.000 steps.

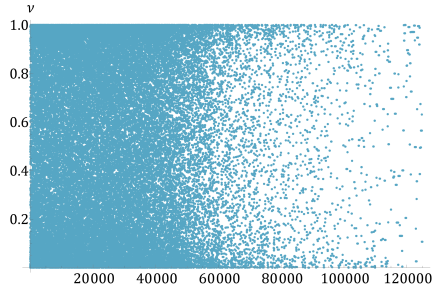

(d) Values for ν per SA step. One run consisted of 125.000 steps.

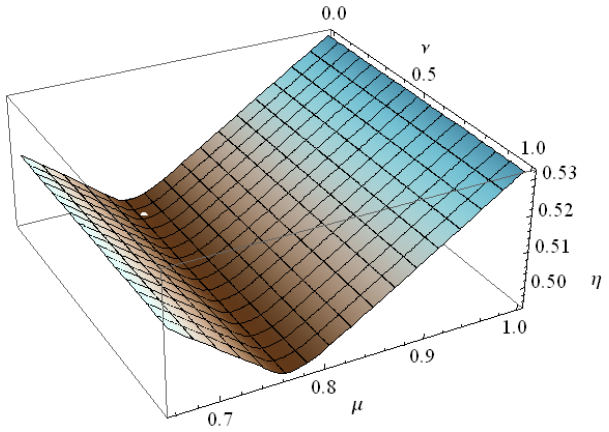

(e) The error η as a function of μ and ν. The white dot indicates the final values that were found for the parameters.

Figure 4.5: Results from fitting the average of the covered area curves of 250 simulations. In the figures, plaques grow linearly.

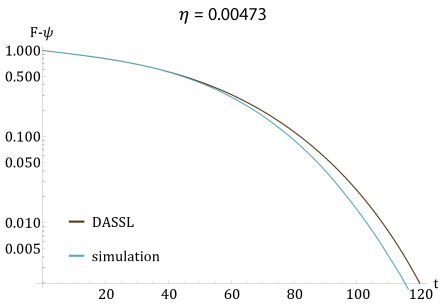

(a) Mean coverage of 250 simulations compared to the optimal curve resulting from the simulated annealing routine

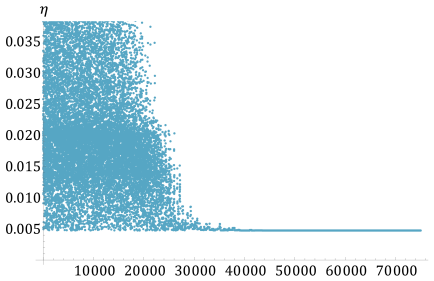

(b) Absolute relative error η per SA step. One run consisted of 125.000 steps.

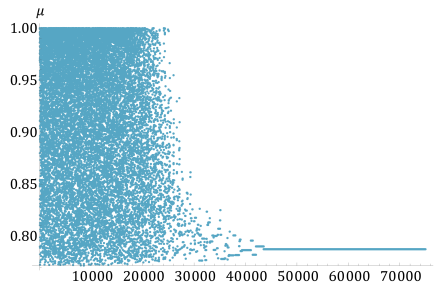

(c) Values for μ per SA step. One run consisted of 125.000 steps.

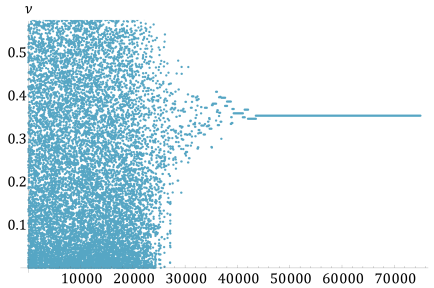

(d) Values for ν per SA step. One run consisted of 125.000 steps.

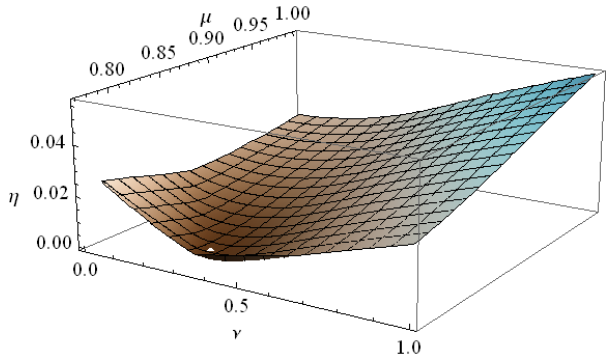

(e) The error η as a function of μ and ν. The white dot indicates the final values that were found for the parameters.

Figure 4.6: Results from fitting the average of the covered area curves of 250 simulations. In the figures, plaques grow quadratically and have a large initial size a_0.

5 Discussion and conclusion

Roughly, this report can be divided into three parts. In Chapter 1 and Chapter 2, an existing mathematical model as presented in [6] is described and analyzed. In Chapter 3, a new model is developed using this early plaque growth model as a starting point. The new model, describing the formation of a necrotic core in plaques is tested and analyzed as well. A problem that arises from fitting experimental data to the original model from [6] is that plaques may overlap. This influences the outcome from the fitting. In Chapter 4, we present a new approach to model plaque growth in mice taking plaque overlap into account. In what follows, we discuss our new results that are presented in Chapter 3 and Chapter 4.

Plaque growth model incorporating apoptosis. Our first new result is a system of differential equations describing the formation of plaques and a necrotic core. In biological literature, many articles about the first stage in plaque growth can be found. However, there is little information about apoptosis and subsequent necrosis. The assumptions that we made when developing the apoptosis model are supported by many articles that we cited. However, research in the future should bring more insight on how the formation of necrotic cores works.

The presented apoptosis model contains a lot of unknown parameters. The number of degrees of freedom is too high to find a unique biological plausible fit to the experimental data. The data that were used only provide plaque sizes and no information about the size of the necrotic cores in the plaques. This means that the results that are discussed in Section 3.2 can only be used as possible scenario's and not as an absolute truth. We conclude that it is possible to find behavior from the model that we consider to be biologically plausible. When more data will be available about necrotic core sizes, the system of equations (3.9) can be used to model core growth. Future experiments might also give insight in the order of magnitude of some of the parameters.

We have shown that it is possible to eliminate one model variable using the quasi steady state approximation if there are large parameter differences. A simple example in the appendix illustrates the idea of quasi steady state approximations and numerical results confirm the fact that the quasi steady state approximation works. Again, more insight in the parameter values is necessary to draw better supported conclusions from the model results.

Overlap model. The overlap model originated from the large size differences of plaques in the data sets. The equations and simulations presented in Chapter 4 are a first effort to model overlapping plaques. In developing the model, we made some rough assumptions. Assuming that plaques grow the same in every mouse might be justified as a start. We should however incorporate the effect of overlap on the growth of plaques, as it does not seem plausible for plaques to continue growing circularly even when they are growing on top of each other. Even though the overlap model has no spatial dependence, it can be improved to account for the changes in growth behavior when plaques start to overlap. As a next step, also the influence of radiation can be incorporated.

In our simulations of growing plaques, we pick a random grid point where a plaque might or might not originate. In every time step after the initiation of a

plaque, we let the plaque-covered regions grow circularly around their initiation points. In this way, it could happen that a small plaque gets completely covered by a much larger plaque if this larger plaque keeps growing. One possible way to take growth changes resulting from overlap into account in the simulations can be implemented as follows. When two plaques start to overlap, there is a grid point that is set to belong to the covered region twice. We could mark these grid points the instant they are covered double and implement a different, slower growth behavior for the marked points. Another possibility is to keep the growth behavior the same for overlapping and non-overlapping plaques but to move the initiation points. By moving the initiation points of overlapping plaques in the opposite direction of where the overlap takes place, the plaques will grow away from each other. Implementing one of these options probably means that the equation describing covered area changes as well.

The final goal of the overlap model is to fit it to data, using possible scenario's for the growth curve that follow from the model (3.9) in Chapter 3. In the maximum likelihood method as explained in Chapter 2, we fitted every plaque separately by computing an expected initiation time. The overlap model however can only be used to fit the total covered area per mouse. This means that more test animals are required in order to gather enough data to find a good fit.

General remarks. The results presented in Chapter 3 and Chapter 4 can be improved but are a good start to model atherosclerosis in mice and the formation of necrotic cores. The numerical error in the numerical simulations and optimizations that were done in both chapters should be analyzed in order to evolve the models. In general, there should be more data available to fit the models and to find well justified results.

Acknowledgment

I express my gratitude to my supervisors Fieke Dekkers and Paul Zegeling. Furthermore, I thank the second reader Tristan van Leeuwen of Utrecht University. I also like to thank my colleagues Teun van Dillen, Astrid Kloosterman and Arjan van Dijk at RIVM for the daily guidance and the many constructive discussions. Last but not least, I thank all colleagues at RIVM for creating a comfortable working atmosphere.

A Illustration of the quasi steady state approximation

We wish to demonstrate the quasi steady state approximation for a simple linear set of differential equations. Take the equations as in (A.1)-(A.2) and assume that $k_1, k_2 \ll k_3$. We will show that solving the equations analytically before imposing the large difference in parameter values yields the same result for $m(t)$ as when we use the quasi steady state approximation.

$$\frac{dm}{dt} = k_1 - k_2 a \tag{A.1}$$

$$\frac{da}{dt} = m - k_3 a \tag{A.2}$$

Analytical solution. Differentiation of (A.1) and substitution gives us the following.

$$\frac{d^2m}{dt^2} = -k_2 \frac{da}{dt} \tag{A.3}$$

$$= -k_2 m + k_2 k_3 a \tag{A.4}$$

$$= -k_2 m - k_3 \frac{dm}{dt} + k_3 k_1 \tag{A.5}$$

We substitute $m(t) = c_1 + c_2 \exp(\lambda t)$ into (A.5).

$$c_2 \lambda^2 e^{\lambda t} = -k_2 c_1 - k_2 c_2 e^{\lambda t} - k_3 c_2 \lambda e^{\lambda t} + k_3 k_1 \tag{A.6}$$

Collecting the exponents gives us a value for c_1 and λ as follows.

$$-k_2 c_1 + k_3 k_1 = 0 \qquad \Rightarrow \qquad c_1 = \frac{k_3 k_1}{k_2} \tag{A.7}$$

$$c_2 e^{\lambda t} \cdot (\lambda^2 + k_3 \lambda + k_2) = 0 \qquad \Rightarrow \qquad \lambda_{1,2} = \frac{-k_3 \pm \sqrt{k_3^2 - 4k_2}}{2} \tag{A.8}$$

Combining the above, we find a new expression for $m(t)$.

$$m(t) = \frac{k_3 k_1}{k_2} + d_1 e^{\lambda_1 t} + d_2 e^{\lambda_2 t} \tag{A.9}$$

The values for d_i can be found by using the initial values $m(0)$ that follows from (A.9) and $\dot{m}(0)$ that follows from (A.9) and (A.1).

$$m_0 - \frac{k_3 k_1}{k_2} = d_1 + d_2 \tag{A.10}$$

$$k_1 - k_2 a_0 = \lambda_1 d_1 + \lambda_2 d_2 \tag{A.11}$$

Subtracting λ_2 times (A.10) from (A.11) gives us a value for d_1.

$$d_1(\lambda_1 - \lambda_2) = k_1 - k_2 a_0 - \lambda_2 m_0 + \lambda_2 \frac{k_3 k_1}{k_2} \tag{A.12}$$

From this expression and (A.10), we can compute d_2.

$$d_2 = m_0 - \frac{k_3 k_1}{k_2} - d_1 \tag{A.13}$$

When imposing $k_3 \gg k_1, k_2$, approximate values for $\lambda_{1,2}$ given by (A.8) can be computed.

$$\lambda_1 \approx -\frac{k_2}{k_3}, \text{ since for } x \text{ small } \sqrt{1-x} \approx 1 - \frac{x}{2} \qquad \lambda_2 \approx -k_3 \tag{A.14}$$

We find

$$\lambda_1 - \lambda_2 \approx k_3 \tag{A.15}$$

which results in the value for d_1 given below.

$$d_1 \approx \frac{1}{k_3}\left(k_1 - k_2 a_0 + k_3 m_0 - k_3 \frac{k_3 k_1}{k_2}\right) \approx m_0 - \frac{k_3 k_1}{k_2} \tag{A.16}$$

Finally, substituting this in (A.13), we find

$$d_2 \approx 0. \tag{A.17}$$

We found the following solution for $m(t)$.

$$m(t) = \frac{k_3 k_1}{k_2} + \left(m_0 - \frac{k_3 k_1}{k_2}\right) e^{-\frac{k_2}{k_3} t} \tag{A.18}$$

Quasi steady state approximation. We state that we can set the time derivative of a to be zero because of the fact that $k_3 \gg k_1, k_2$. We find the following dependence for a.

$$\frac{da}{dt} = m - k_3 a = 0 \qquad \Rightarrow \qquad a = \frac{m}{k_3} \tag{A.19}$$

Substitute this expression in (A.1).

$$\frac{dm}{dt} = k_1 - k_2 \frac{m}{k_3} \tag{A.20}$$

The equation for $m(t)$ that follows is

$$m(t) = \left(m_0 - \frac{k_3 k_1}{k_2}\right) e^{-\frac{k_2}{k_3} t} + \frac{k_3 k_1}{k_2} \tag{A.21}$$

which equals the equation given in (A.18).

We conclude that, when considering the slow variable m, we can use the quasi steady state approximation for the fast variable a.

B Terminology

Apoptosis
Form of cell death, induced by the cell itself. The cell falls apart in fragments (apoptotic bodies), surrounded by a membrane and filled with cell content. No cell content is spilled.

Apoptotic body
See apoptosis.

Cytokines
General name for small proteins released by cells. They regulate all kinds of processes by communicating between cells. In atherosclerosis, they regulate the recruitment of macrophages.

Endothelium
Layer between the bloodstream and the artery wall, only one cell thick.

Foam cell
Loaded macrophage, completely filled up by LDL particles.

Intima
Inner layer of the artery wall, closest to the bloodstream.

LDL
Low-density lipoprotein. Structures filled with lipid that is transferred from and to the organs through the blood.

Lumen
Bloodstream.

Macrophage
Type of white blood cell that cleans unwanted material by engulfing it. The cleaning is an inflammatory process.

Necrotic core
Cellular debris that is spilled in the center of a plaque after secondary necrosis. Usually only detectable in advanced plaques. See secondary necrosis.

Phagocytosis
The engulfing of (unwanted) particles by a macrophage.

ROS
Reactive oxygen species. Reactive molecules and free radicals derived from molecular oxygen that are a potential cause of damage to cells.

Secondary necrosis
Form of cell death that happens to apoptotic bodies when they are not cleared fast enough. The apoptotic body breaks up and its content is spilled in the plaque, forming a necrotic core.

T-cell
Type of white blood cell that regulates inflammatory reactions by reacting to cytokines.

Bibliography

[1] CA Cobbold, JA Sherratt, and SRJ Maxwell. Lipoprotein oxidation and its significance for atherosclerosis: a mathematical approach. *Bulletin of Mathematical Biology*, 64(1):65–95, 2002.

[2] O Diekmann, H Heesterbeek, and T Britton. *Mathematical Tools for Understanding Infectious Disease Dynamics*. Princeton University Press, 2012.

[3] JJ Duistermaat and W Eckhaus. *Analyse van Gewone Differentiaalvergelijkingen*. Epsilon Uitgaven, second edition, 2001.

[4] S Hoving et al. Single-dose and fractionated irradiation promote initiation and progression of atherosclerosis and induce an inflammatory plaque phenotyp in apoe -/- mice. *International Journal of Radiation Oncology Biology Physics*, 71(3):848–857, 2008.

[5] L Ingber. Simulated annealing: Practice versus theory. *Mathematical and Computer Modelling*, 18(11):29–57, 1993.

[6] A Kloosterman, T van Dillen, et al. How radiation influences atherosclerotic plaque development; a biophysical approach in mice. (to be submitted).

[7] Z Mallat and A Tedgui. Apoptosis in the vasculature: Mechanisms and functional importance. *British Journal of Pharmacology*, 130(5):947–962, 2000.

[8] M Mancuso et al. Acceleration of atherogenesis in apoe(-/-) mice exposed to acute or low-dose-rate ionizing radiation. *Oncotarget*, 6(31):31263–31271, 2015.

[9] REJ Mitchel et al. Low-dose radiation exposure and atherosclerosis in apoe(-/-) mice. *Radiation Research*, 175(5):665–676, 2011.

[10] A Ougrinovskaia, RS Thompson, and MR Myerscough. An ode model of early stages of atherosclerosis: Mechanisms of the inflammatory response. *Bulletin of Mathematical Biology*, 72(6):1534–1561, 2010.

[11] LR Petzold. A description of dassl: A differential/algebraic system solver. In *Proc. IMACS World Congress*, pages 430–432, 1982.

[12] R Salvayre et al. Oxidized low-density lipoprotein-induced apoptosis. *Biochimica et Biophysica Acta*, 1585:213–221, 2002.

[13] A Saraste and K Pulkki. Morphologic and biochemical hallmarks of apoptosis. *Cardiovascular Research*, 45(3):528–537, 2000.

[14] DM Schrijvers et al. Phagocytosis of apoptotic cells by macrophages is impaired in atherosclerosis. *Arteriosclerosis Thrombosis and Vascular Biology*, 25(6):1256–1261, 2005.

[15] DM Schrijvers et al. Phagocytosis in atherosclerosis: Molecular mechanisms and implications for plaque progression and stability. *Cardiovascular Research*, 73(3):470–480, 2007.

[16] T Seimon and I Tabas. Mechanisms and consequences of macrophage apoptosis in atherosclerosis. *Journal of Lipid Research*, 50:S382–S387, 2009.

[17] Y Shimizu et al. Radiation exposure and circulatory disease risk: Hiroshima and nagasaki atomic bomb survivor data, 1950-2003. *British Medical Journal*, 340, 2010.

[18] FA Stewart, S Hoving, and NS Russell. Vascular damage as an underlying mechanism of cardiac and cerebral toxicity in irradiated cancer patients. *Radiation Research*, 174:865–869, 2010.